



# UNIVERSITY OF PAVIA

PHYSICS DEPARTMENT

MASTER'S DEGREE COURSE IN PHYSICAL SCIENCES



A GEANT4 TOOLKIT TO SIMULATE X-RAYS  
TUBES FOR RADIOBIOLOGICAL EXPERIMENTS

UN TOOLKIT GEANT4 PER LA SIMULAZIONE DI  
TUBI A RAGGI X PER ESPERIMENTI  
RADIOBIOLOGICI

Supervisor:

Dr. Ian Postuma

Co-supervisor:

Prof. Silva Bortolussi

Thesis written by:

Santa Gabriella Bonaccorsi

Academic year 2021/2022

# Contents

<b>Abstract</b>	<b>4</b>
<b>Abstract (Italian Version)</b>	<b>7</b>
<b>Introduction</b>	<b>8</b>
<b>1 Theoretical Background</b>	<b>10</b>
1.1 Introduction of ionizing radiation . . . . .	10
1.1.1 The X-Ray . . . . .	10
1.2 Radiation-matter interaction . . . . .	13
1.2.1 The cell and the DNA . . . . .	15
1.2.2 Radiobiology . . . . .	16
1.2.3 DNA damages . . . . .	18
1.3 Monte Carlo codes . . . . .	19
1.3.1 Condensed History and Truck Structure Codes . . . . .	21
1.4 GEANT4: A brief introduction . . . . .	21
1.4.1 Software architecture . . . . .	23
1.4.2 GEANT4 examples . . . . .	23
1.5 GEANT4-DNA: the GEANT4 extension to simulate DNA damages	26
1.5.1 Key package features . . . . .	28
1.5.2 How to model a track structure . . . . .	28
1.5.3 The Geometry in GEANT4-DNA . . . . .	31
<b>2 Materials and methods</b>	<b>36</b>
2.1 The experimental configuration . . . . .	36
2.1.1 The X-ray Tube . . . . .	36
2.1.2 The experimental set up . . . . .	36
2.1.3 The RADCAL Camera . . . . .	38
2.1.4 The experimental data . . . . .	38
2.2 Simulation of the photon energy spectrum . . . . .	40
2.3 The available class for Geant4 XRayTube code development . . .	41
2.3.1 The Geometry . . . . .	41
2.3.2 The Physics List . . . . .	41
2.3.3 The Source . . . . .	42
2.3.4 The Scoring . . . . .	42

<i>CONTENTS</i>	3
<b>3 Results</b>	<b>44</b>
3.1 Geometry construction and approximations . . . . .	44
3.1.1 Source construction and approximation . . . . .	47
3.1.2 The physics list . . . . .	47
3.2 Analysis . . . . .	50
3.2.1 The photon spectrum . . . . .	50
3.2.2 Consideration on the calibration . . . . .	51
<b>4 Experimental irradiation for DNA damages studies with the foci technique</b>	<b>54</b>
4.1 The foci technique . . . . .	54
4.2 The experimental set-up . . . . .	55
4.2.1 Preliminary phase . . . . .	55
4.2.2 The irradiation . . . . .	55
4.2.3 Protocol application . . . . .	56
4.3 Experimental Results . . . . .	59
<b>5 Conclusions and future perspectives</b>	<b>62</b>
<b>Ringraziamenti</b>	<b>64</b>

# Abstract

Monte Carlo simulation codes are widely used in scientific research as they make a crucial contribution to the simulation of large amounts of data, returning reliable and often predictive results. Among these, GEANT4 is one of the toolkits that is used for simulations in fields where radiation-matter interaction plays an important role, e.g. high-energy or medical physics. In this work, GEANT4 was used to simulate an X-ray tube for radiobiological experiments.

X-ray tubes are now widely used both in medical contexts, e.g. in radiology or radiotherapy applications, and in research contexts, for radiobiological experiments. To conduct such experiments, however, it is necessary to have a good knowledge of the characteristics of the X-ray beam used, which include its energy spectrum, intensity and spatial distribution. However, measuring these characteristics can be difficult and time-consuming, especially for experiments requiring a high degree of precision and reproducibility.

To overcome these obstacles, Monte Carlo simulations become a valuable tool, and GEANT4 is a powerful and flexible simulation toolkit, capable of simulating the production of X-rays in detail, allowing the geometry of the system, the material properties of the components used and the energy and direction of the source particles to be defined.

For this work, the simulation of the X-ray tube began by defining its geometry, a vacuum tube with a tungsten anode and a copper filter. Next, the electron source was implemented inside the tube, defining its energy, momentum and direction of the emitted electrons and the physics for reproducing the X-ray beam.

The aim of the work was to use this X-ray tube to reproduce the experimental set-up of a radiobiological irradiation carried out at the University of Naples: to this end, two configurations were implemented. The first simulation was used to carry out a validation of the dose obtained from the calibration performed by a Radcal ionisation chamber. The second simulation calculated the dosimetry in a single-cell layer. The results obtained are part of a broader research project in the field of BNCT, in which this toolkit will become the tool for further simulation. It will allow performing dose-effect simulation at the sub-cellular level, not only for with X-rays irradiation but also for the mixed radiation field of BNCT.



# Abstract (Italian Version)

I software di simulazione Monte Carlo sono ampiamente utilizzati nell'ambito della ricerca scientifica poichè offrono un contributo determinante per la simulazione di grandi quantità di dati, restituendo risultati affidabili e, spesso, predittivi. Tra questi, GEANT4 è uno dei toolkit che viene utilizzato per simulazioni nei campi in cui l'interazione radiazione materia gioca un ruolo importante, ad esempio nella fisica delle alte energie o in fisica medica. In questo lavoro GEANT4 è stato utilizzato per simulare un tubo a raggi X per esperimenti radiobiologici.

I tubi a raggi X ad oggi trovano largo impiego sia in contesti medici, ad esempio in applicazioni di radiologia o radioterapia, sia in contesti di ricerca, per esperimenti radiobiologici. Per condurre tali esperimenti è però necessario possedere una buona conoscenza delle caratteristiche del fascio di raggi X utilizzato, come lo spettro di energia, l'intensità e la distribuzione spaziale. Tuttavia, la misura di queste caratteristiche può essere complesso, specialmente per gli esperimenti che richiedono un elevato grado di precisione e riproducibilità.

Per superare questi ostacoli, le simulazioni Monte Carlo diventano un valido strumento e GEANT4 è un toolkit di simulazione potente e flessibile, in grado di simulare nel dettaglio la produzione dei raggi X, permettendo di definire la geometria del sistema, le proprietà dei materiali dei componenti utilizzati e l'energia e la direzione di volo delle particelle emesse dalla sorgente. Per questo lavoro, la simulazione del tubo a raggi X è iniziata definendone la geometria: un tubo a vuoto con un anodo in tungsteno e un filtro in rame. Successivamente è stata implementata la sorgente di elettroni, posta ancora dentro il tubo, della quale è stato possibile definire energia, momento e direzione degli elettroni emessi e la fisica per la riproduzione del fascio di raggi X.

L'obiettivo del lavoro è stato quello di utilizzare questo tubo radiogeno per riprodurre lo spettro di un irraggiamento radiobiologico svolto presso l'università degli studi di Napoli. A tal fine sono state implementate due configurazioni: la prima per effettuare una validazione della dose ottenuta dalla calibrazione effettuata da una camera a ionizzazione Radcal e una seconda in cui si sono effettuati studi di dosimetria su uno strato monocellulare di tessuto soffice. I risultati ottenuti si inquadrano nell'ottica molto più ampia di un progetto di

ricerca in ambito BNCT in cui questo toolkit diventerà uno strumento utile non solo per le simulazioni future di irraggiamenti con raggi X ma anche per il campo misto di radiazione tipico dell'irraggiamento neutronico per BNCT.

# Introduction

The Boron Neutron Capture Therapy, or BNCT, is an experimental therapy for the treatment of metastatic cancer that uses a binary approach: the treatment first consists of administering to patients a borated formulation able to achieve a higher concentration in the tumour cells compared to the normal ones. Then, the tumour target is irradiated with an epithermal neutrons beam that, once penetrated into the tissue, thermalises. At thermal energy, the cross section of neutron capture in  $^{10}\text{B}$  is maximum, according to the reaction (1)



The results of boron-neutron interaction is the production of alpha particles and lithium ions which have a high LET and a range comparable to the cell dimension, a few micrometers. These particles cause a damage that can be lethal for tumour cells, providing a suitable intra-cellular boron concentration and a sufficient neutron fluence.

The possibility to destroy the tumour without affecting the functionality of normal tissues depends on the boron selectivity obtained with the borated drug. The effectiveness of the therapy also depends on the boron localization inside the cells: if it is closer to the DNA, the biological effect can be enhanced. Effectiveness of BNCT is typically studied in vitro by building dose-response curves. Simulating these curves is a complex operation because the total dose deposited in tissues is not only due to boron capture, there are other contributions that must be take into account.

Specifically, in a biological tissues, a neutron interacts, depending on its energy, with nitrogen, producing a proton (of about 600 keV energy) and with hydrogen, producing 2.2 MeV photons. Moreover, in the thermalisation process, epithermal neutrons lose their energy by elastic scattering in hydrogen, which deposit dose via proton recoil.

In addition there is a gamma contribution due to photons present in the beam and generated by the interaction of neutrons with the materials of the facility. For this reason, BNCT dosimetry must be carefully calculated by Monte Carlo in order to understand how an organism responds to a mixed field. Studies in culture cells (millimeter scale) were performed for different cell cultures [1]: dose was calculated and cell survival curves were obtained with the best possible precision.

Increasing the granularity, it is interesting to study how cell damages occur and

evolve due to the boron localization in a nanometer scale. Measurement and simulations must be performed for BNCT, for neutron irradiation only and for photon irradiation as a reference. These results, in fact, are expected to deepen the insight into the relation between absorbed dose and biological effect, with the final goal to improve the BNCT dose prescription and capacity of predicting the clinical outcome given the in-patient dose distribution.

This work contributes to a better understanding of dosimetry in BNCT. It has been developed in the frame of a project whose goal is to study the DNA damage, both experimentally and by simulations, useful to make predictions on the effectiveness of the therapy given a certain boron distribution in cell. To this end, new computational instruments have been employed.

The use of the Open Source toolkit Geant4, represents the first step of intracellular dose calculation and simulation of the effects. From the point of view of experimental measurements, new biological essays and techniques were explored, in addition to the evaluation of cell survival and clonogenicity already available in the research group. To this end, a new collaboration with the Biophysics group of University of Naples has been recently started. Cultures of UMR106 cell line [2] were prepared to evaluate DNA damages by the use of a foci technique after irradiation. These cells have been extensively used in Pavia for previous BNCT studies [3].

This thesis represents the initial steps in learning how the code works, and how it can be used for these purposes. The first experiments have been performed with the reference radiation: an X-ray source located in Naples. Geant4 was thus used to reproduce these experiments. The result of the work consists in the construction of a tool able to simulate a set-up for X-ray irradiation. This tool, in the near future, will be used as the input to study DNA damages in cells.

The thesis is divided into five chapters: the first reports the theoretical background about interaction of radiation in biological matter and its effects. Moreover, it introduces the Geant4 code capabilities and features. Finally, it describes the Geant4-DNA code, developed to simulate the DNA damage.

The second Chapter is devoted to the description of the experimental irradiation set-up at the University of Naples, with a brief overview of the instruments employed in this work. It also describes all the objects, classes and methods involved in the development of the code and offers a different tool for validating the expected result.

The third Chapter shows the final structure of the code: the geometry, the shape and characteristics of the particle source and the implemented physics. The final results are also introduced and analysed.

The fourth Chapter enters into an experimental perspective and reports on the experience of the cell irradiation carried out in Naples in November 2022, showing some preliminary results.

Finally, the fifth Chapter summarizes the contributions of this work to the current research and casts an overview of how it fits into a broader perspective.

# Chapter 1

## Theoretical Background

### 1.1 Introduction of ionizing radiation

Researching in the radiation physics field has started after the realization of the first radiography of Mrs Roentgen's hand by Mister Roentgen in 1895. The remarkable impact of this publication in medical field subsequently has lead scientist to achieve other important goals such as Becquerel's studies on radioactive decay and Miss and Mister Curie's discovery of radium.

Today, the concept of **ionizing radiation** describes types of radiation capable of carrying more, or at least the same amount of energy to ionise the matter and they can be classified into two groups: directly and indirectly ionising radiation, to distinguish their different ability to directly or indirectly excite and ionise the atoms of matter with which they interact.

Particles such as electrons, positrons, or ions, like the alpha or heavier ones, are directly ionizing radiations, actually they able to penetrate matter according to their energy and physical properties. Due to Coulomb-force-interaction which just occurring during the particle tracks through matter [4], they are able to strip matter of its electrons, protons or ions. This effect causes an instantaneous rearrangement of the target system which might result in a change of properties. Neutrons and photons, on the other hand, are called indirect ionizing radiation because they deposit their energy along their tracks by interacting with other charged particles called *secondaries*. It is the secondaries that are ultimately responsible for inducing chemical reactions and/or initiating other physical processes possibly changing the chemical and physical properties of the targets.

Actually, to strip an electron from matter, the energy required is about  $4 - 25eV$  which means that, considering the entire spectrum of electromagnetic waves, only X-ray and gamma particles have the right amount of energy to ionise matter [4] instead, electromagnetic waves with energy equal to or less than that of UV rays are called non-ionising radiation.

#### 1.1.1 The X-Ray

Electromagnetic waves with a wavelength between  $10^{-11}$  and  $10^{-9}m$  are called X-Rays.

### The X-Ray tube

The devices producing X-rays are the X-rays tubes and they are widely used in the medical field for imaging by radiography, CT scan or radiotherapy treatments.

The tube Fig. 1.1 consists of a vacuum cup externally covered in metal, usually lead is preferred, and of two electrodes: the cathode and the anode. The cathode is a metal filament made usually of copper, inserted inside a focusing cup. The anode consists in a foil made of a metallic material with a high atomic number  $Z$ .

Two different supply circuits are required for its operation: a first one connected to the cathode, which generates a DC voltage, and a second one capable of establishing a potential difference between the cathode and the anode. The physical process exploited is the *thermoionic effect*: the cathode is heated by the current generator until the electron ionization threshold is exceeded. At this point, the produced electrons are focused and accelerated thanks to the presence of the electric field generated by the second power circuit, and go straight on the focal spot of the anode.

Here, some physical interactions occurs between electrons and anode's atoms, which will be better described in the paragraph below, and a lot of X-ray were produced. Then, the X-ray beam exits the tube through a glass window inserted in the machine, but in X-ray tubes used for diagnostics, only 1% of the X-rays produced exit the window, the remaining percentage being converted into energy as it hits the target [4].

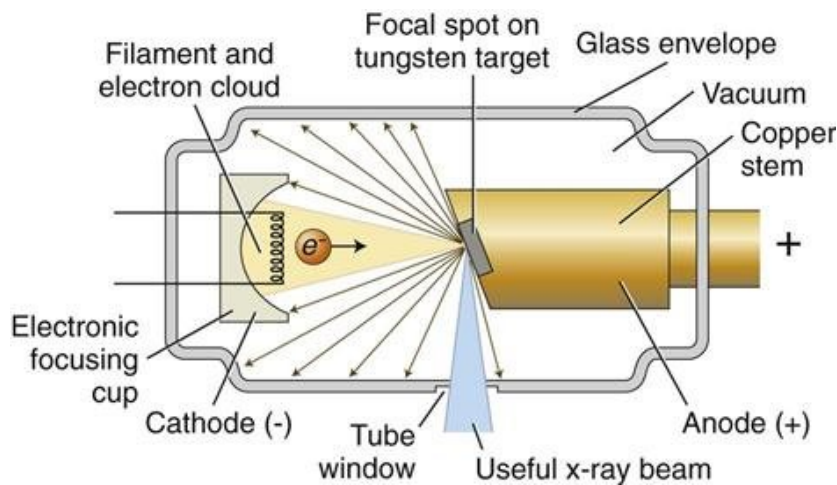


Figure 1.1: Conventional representation of a common X-ray tube and emitted electrons [5]

### The X-Rays Production

The production of the X-ray beam from the anode is made possible by two different processes that occur during the electron impact: the Bremsstrahlung effect and the emission of characteristic X-rays.

When the electrons are directed towards the target, the high atomic number  $Z$  of

the tungsten decelerates them and the occurring radiative loss can be described by the Eq. ( 1.1), where it is important to emphasise the  $Z^2$  dependence

$$\left(\frac{dE}{\rho dX}\right)_{rad} = \alpha_0 \frac{NZ^2}{A} (E + m_0c^2)B. \quad (1.1)$$

When an electron crosses the tungsten electronic shells and arrives near the nucleus, it is affected by the local electric field and it is deflected from its original trajectory. The change in direction causes the electron to lose its kinetic energy and, according to the principle of energy conservation, a photon in the X-ray range is produced; this radiative loss is called the *Bremsstrahlung effect* in German.

With a classical physics description, if  $v_1$  is the electron velocity and  $E_1$  is its kinetic energy, after the change of direction, the electron will have a velocity  $v_2$  and a kinetic energy  $E_2$ . The emitted photon therefore will have a wavelength that depends on the difference between  $E_1$  and  $E_2$

$$\lambda = hf = E_2 - E_1 \quad (1.2)$$

where  $h$  is the Plank constant and  $f$  the frequency. The concurrent physical process is called *characteristic X-rays production*.

Sometimes an electron collides with another electron which belongs different tungsten shells, for example the K-shell, releasing his energy in the scattering and causing ionization processes if its energy is exactly the same or higher than the electronic shell energy. In this case, the atom loses one of his K-shell electrons creating a gap. In order to minimize the atom energy, an electron from the closest shell, the L-shell, replaces the lacuna and a X-ray is emitted with energy equal to the difference of the binding energies of the two shells. Thus the energy is equal to

$$E_{x-ray} = E_K - E_L \quad (1.3)$$

and the transition is called  $k_\alpha$ . If the replacement occurred from shell M to the K-shell, the name would be  $k_\beta$ , and so on.

These two different processes also have different cross sections than the Bremsstrahlung effect, in particular, the atom energy loss cross section depends on  $\frac{1}{m^2}$ , therefore smaller the mass of the interacting particle larger will be the probability of the Bremsstrahlung effect.

The atomic number  $Z$  of the target also plays an important role: it defines the amount of X-rays produced by Bremsstrahlung, as pointed out above, in Eq. ( 1.1) and the quality of the beam in terms of the production of characteristic X-rays. In the typical diagnostic X-rays tubes, about the 80% of X-rays are produced by the Bremsstrahlung effect [4].

### The X-Rays Spectra

The emission spectrum from a X-ray tube has the characteristic shape shown in Fig. 1.2.

The area under the continuous line in the graph 1.2 is called photon intensity  $I$  and it is proportional to both the square of the supply Voltage of the tube  $V$  and the current intensity  $i$ , as expressed in the Eq. ( 1.4)

$$I = V^2 * i. \quad (1.4)$$

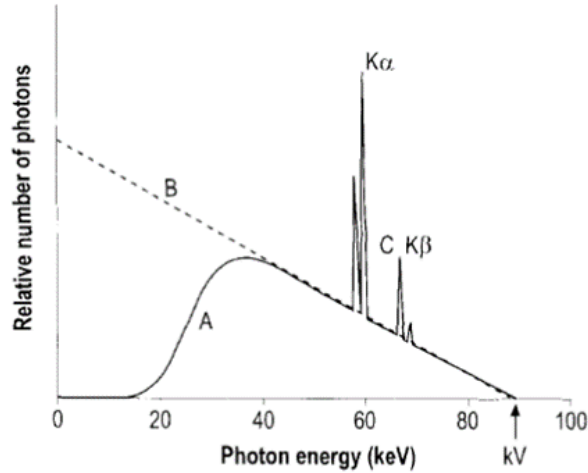


Figure 1.2: X-rays spectrum from a X-ray tube with a tungsten anode [4]. The plot shows the number of emitted photons as a function the photon energy in keV. The spectrum (A) is the results of the overlap of two different contributes: the continuous Bremsstrahlung spectrum (B) and the stripped spectrum of the characteristic X-rays emission (C). However the A shape depends also by the filtration contribute.

The maximum energy of the photon spectrum depends on the kinetic energy of the electrons emitted by the cathode, which in turn depends on the tube voltage. The minimum energy of the produced photons can be zero, but the minimum energy with which the photons escape from the tube depends on other factors such as the filtration of the tube and it is never zero.

The total filtration is due to two filtration contributes called *inherent* and *additional*. The inherent filtration is related to the machine construction parameters and it is responsible for the X-ray absorption in the walls of the tube, when they are produced at low energies. The additional one depends on filters that may be added externally to the window, through which the X-ray beam must necessarily pass: in this way, a beam with a defined minimum energy threshold is obtained. For this reason, It is possible to define a parameter named *tube efficiency*  $\epsilon$  that characterises the machine: it is equal to the ratio between the intensity  $I$  of the emitted photons and the electrical power applied to the tube  $V$  Eq. ( 1.5)

$$\epsilon = \frac{I}{V}. \quad (1.5)$$

## 1.2 Radiation-matter interaction

The passage of radiation through matter can cause ionisation and/or excitation that can change its chemical and physical properties, as anticipated above.

Photons interact with matter in three different ways: the *photoelectric effect*, *Compton scattering* and *pair production* processes.

The parameter that quantifies the probability of an interaction occurring is the

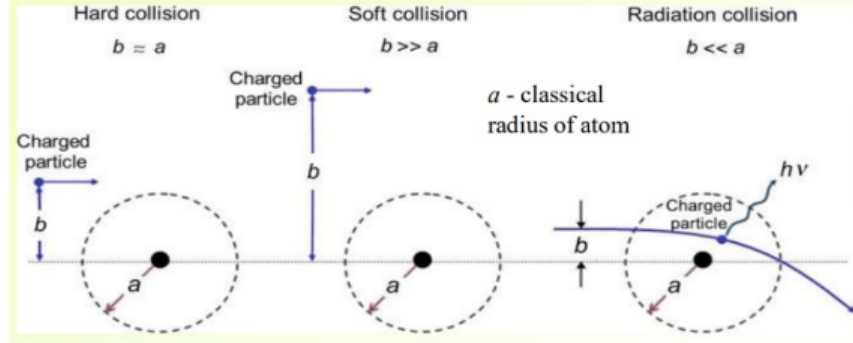


Figure 1.3: Types of Collisions according to the impact parameter  $b$

cross section  $\sigma$ . For photons, the total probability of interaction is the sum of the cross sections associated with each process Eq. ( 1.6)

$$\sigma_{tot} = \sigma_{\gamma} + \sigma_c + \sigma_{pp}. \quad (1.6)$$

The cross sections depend on the atomic number of the target  $Z$  and the energy of the incident photon  $E$  [4]

- *photoelectric*  $\sigma_{\gamma} \propto \frac{Z^n}{E^m}$  where  $n=4 \div 4.5$  and  $m=3 \div 3.5$
- *Compton*  $\sigma_c \propto \frac{Z}{E}$
- *pair production*  $\sigma_{pp} \propto Z^2 * \ln(E + cost)$

The cross section is also related to the linear attenuation coefficient, which measures the ability of matter to attenuate the radiation beam as a function of its atomic number. The linear mass attenuation coefficient defined as  $\frac{\mu}{\rho}$  is often used to eliminate the dependence on the density of matter.

The interaction probability in the case of charged particles with matter can instead be determined by including the size dependence of the *impact parameter*  $b$  in the cross section. The impact parameter  $b$  corresponds to the length of the segment orthogonally joining the trajectory of the projectile with the position of the target nucleus, i.e. from the point of origin of the force field felt by the incident particle. The type of collision can be predicted as a function of the ratio of the size of the impact parameter to the atomic radius  $a$  of the target nucleus [4], for examples:

- *Hard collisions*: when  $b = a$ , scattering generally occurs between the particle and an atomic electron that will be ejected producing delta rays [4].
- *Soft collisions*: when  $b \gg a$  the collision is called soft because the coulomb force between the charged particles and the nucleus is mediated over the entire atom and the results are ionisation and excitation [4].

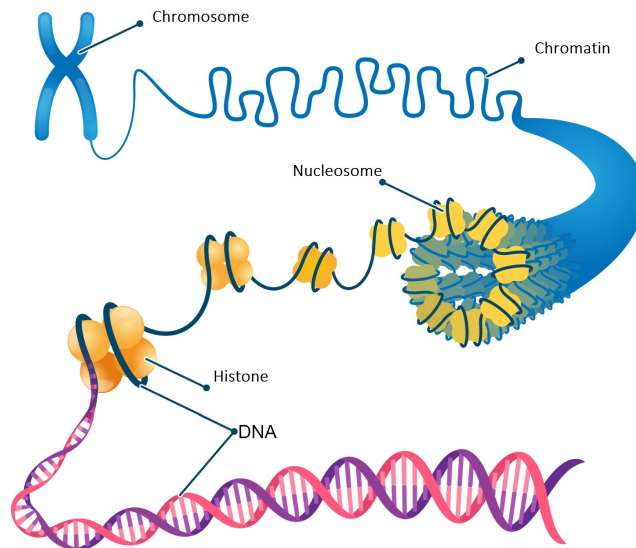


Figure 1.4: The five compaction levels of DNA molecule [8]

### 1.2.1 The cell and the DNA

When the target of radiation is a biological system such as a living cell, the changes caused by radiation can be significant and sometimes decisive for its proper functioning.

The cell is classified as the smallest living structure, capable of creating offspring and surviving on its own. It is the fundamental unit that constitute all the living biological systems, such as the human being. The internal structure of the cell differs in *prokaryotic* and *eukaryotic* organisms in that the nucleus is only in the latter enclosed within a membrane. Human cells are all eukaryotic and the characteristics described below apply only to these.

Even inside the same living system, cells may differ from one another due to their level of differentiation and the role they play within the tissue they belong, but into their nucleus there is always a particular molecule called DNA.

DNA is characterised by a double helix structure, each characterised by phosphate groups that make up its skeleton [6], nitrogenous bases and deoxyribose sugar; its key role is to preserve all the genetic information that allows the system to develop, function properly and reproduce [7].

The connection between a nitrogenous base, deoxyribose and a phosphate group is called nucleotide and, given the presence of 4 different bases such as adenine, thymine, guanine and cytosine, it is possible to distinguish 4 types of nucleotides. DNA is 2 metres long, but it fits inside a nucleus that has a radius of 10 nm. Its structure is actually very ductile: its shape can take on different configurations, compacting or unwinding depending on the phase of the cell life cycle. For example, during the cell duplication phase, DNA organises itself into 23 other small pairs of molecules called chromosomes.

Fig. 1.4 shows the five levels of DNA compaction: the first level is where the DNA coils along spheroid-shaped proteins called histones that prevent the DNA

to tangle, these structures connect to each other to form nucleosomes. When the nucleosomes compact again into  $30\text{ nm}$  long structures thanks to *linkers* ( $20\text{ bps}$  long structures), the DNA takes on the characteristic shape called pearl necklace. In the fourth level of compaction, the DNA forms chromatin, evenly distributed throughout the nucleus, which can still fold back on itself to form loops during the duplication stages, in which the DNA splits into chromosomes.

## 1.2.2 Radiobiology

When ionising radiation hits the DNA molecule, the outcome can never be predicted with 100% certainty because it depends on the type of damage induced and where the structure is struck.

One of the most important physical quantities used in order to quantify the radiation damages is the Dose, defined as the energy deposited by radiation per unit mass

$$D = \frac{dE}{dm}. \quad (1.7)$$

Radiobiology is the discipline that studies the biological effect of ionising radiation taking into account even the quantity of dose received by biological systems. Radiobiologists describe the processes occurring after a biological system irradiation and organise them on a time scale, enclosing more than 20 orders of magnitude (as illustrated in the Fig. 1.5 below), in distinguish phases which are:

- **Physical stage** occurring between  $10^{-15}$  and  $10^{-12}\text{ s}$  : it is when the radiation deposits energy in the biological target and the first physical phenomena such as excitation or direct ionisation happen;
- **Physico-chemical stages** starting from  $10^{-12}\text{ s}$  and ending before  $1\text{ ms}$ : the energy deposited in the previous stage often causes the dissociation of water molecules and consequently the production of ions and free radicals, which can either recombine or diffuse inside the nucleus causing further ionisation or visible DNA damage;
- **Biological Phases** begin in about  $1\text{ ms}$ : DNA damage becomes visible and the cell recognises and tries to repair it by activating natural mechanisms. Enzymes and proteins act in synchrony to fix the breaks or to induce the cell to start an apoptosis path.

One second after the irradiation the cell is either dead or it can go through a series of reactions which determine transformations such as mutation and/or chromosome aberration which can be seen in one hour. In a few cases, the mutated cell may be able to reproduce and to generate a cancerous disease. Otherwise, the mutation may remain silent for years or be passed genetically to the offspring of the biological system. In these cases, the mutation can display an impact even after more than 50 years. A simplified scheme is shown in Fig. 1.6.

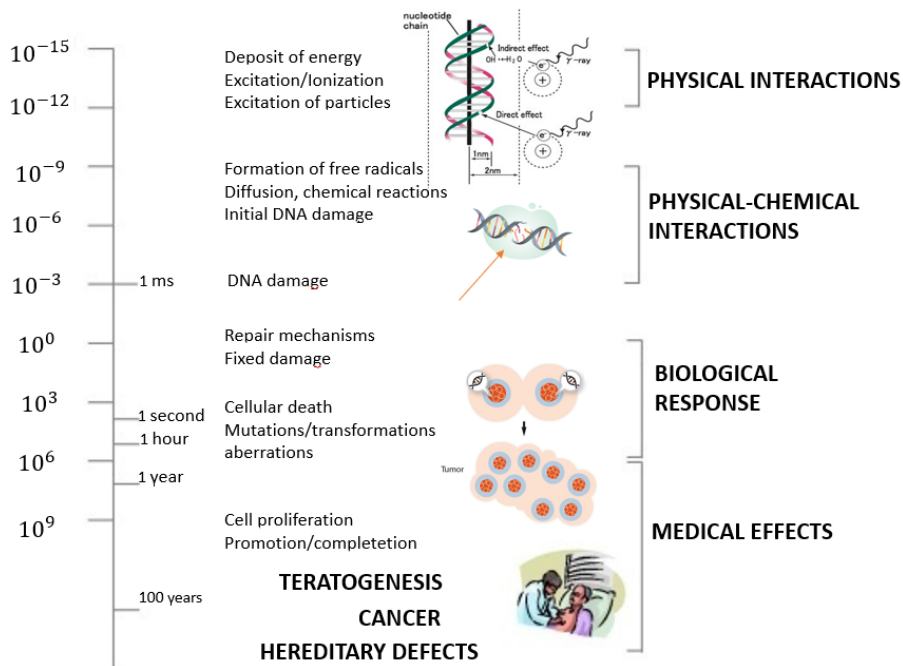


Figure 1.5: Time scale for generate DNA damages by ionising radiation [9]

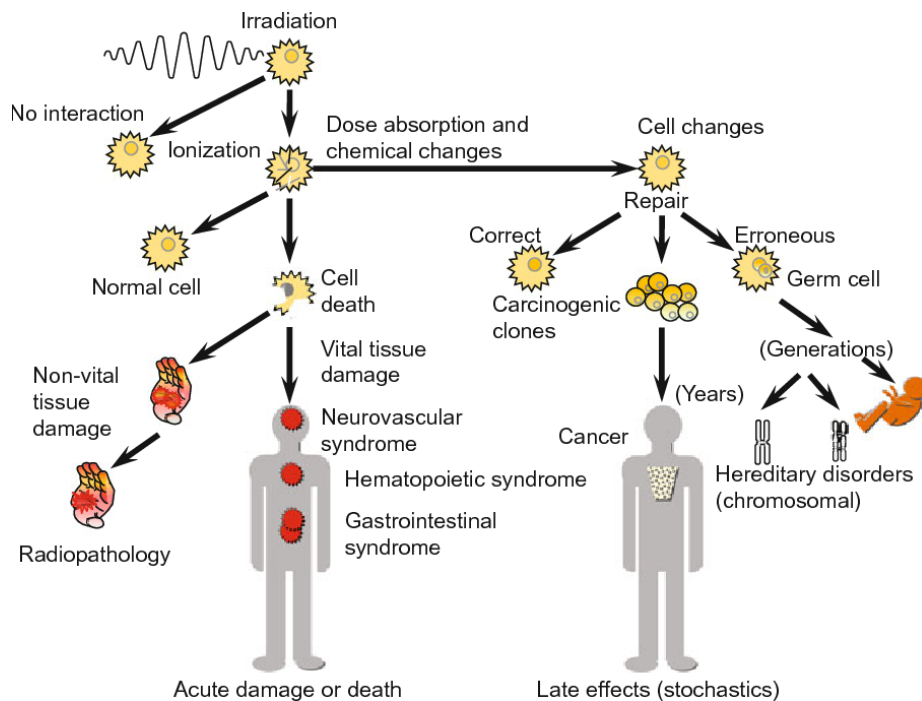


Figure 1.6: Possible biological effects due to irradiation by ionizing radiations [10]

### 1.2.3 DNA damages

The radiation can act by causing a break at a single point in the DNA helix, involving the bonds between the nitrogenous base, deoxyribose sugar or phosphate group, in which case the damage is called *Single Strand Break SSB*. In most cases, the cell is able to successfully repair this type of damage by mechanisms that use the healthy brother chromatids as copies.

When interactions cause damage involving both helices and it happens that two *SSBs* occur at a distance lower than 10 *pbs*, the damage is called *Double Strand Break DSB* and the repair mechanisms are different than before, because there is no longer a healthy helix to be used as a copy.

This is why sometimes the success of the repair is not guaranteed and chromosomal aberrations can be produced that can be either fatal for the cell or transform it in a mutated, potentially harmful cell.

If there are more than two damages within the 10 *pbs* range, we speak of *damage clusters*.

In order to consider the ability of radiation to induce a specific damage, two parameters are used in radiobiology: the **LET**, linear energy transfer, and the **RBE**, relative biological effectiveness.

The LET Eq. ( 1.8) of a charged particle defines the value of energy that the radiation loses per unit path and depends on the atomic number  $Z$ , the atomic mass  $A$  and the density of target, the square of the particle atomic number  $z^2$  and the inverse of the square of its velocity  $v^2$  (in Eq. ( 1.8)  $\beta = \frac{v}{c}$  where  $c$  is the speed of light)

$$\frac{dE}{dx} \propto \rho \frac{Z z^2}{A \beta^2}. \quad (1.8)$$

The RBE Eq.( 1.9) of a particle is a parameter that is used to characterise a radiation from the point of view of the biological damage caused in comparison to a reference radiation (usually photons). It is equal to the ratio of the dose value deposited by the reference radiation to achieve a specific biological endpoint, and the dose value required by another radiation to achieve the same endpoint.

$$RBE = \frac{D_X}{D_{radiation}} \quad (1.9)$$

LET and RBE are related quantities: the higher the LET of a particle, the higher its RBE and thus the greater its biological effect compared to that of photons.

This relationship, however, is not always valid because above a certain LET, the phenomenon of *overkilling* occurs Fig. 1.7: as the maximum effect has already been caused (i.e. cell death), an increase of LET does not imply any further biological damage.

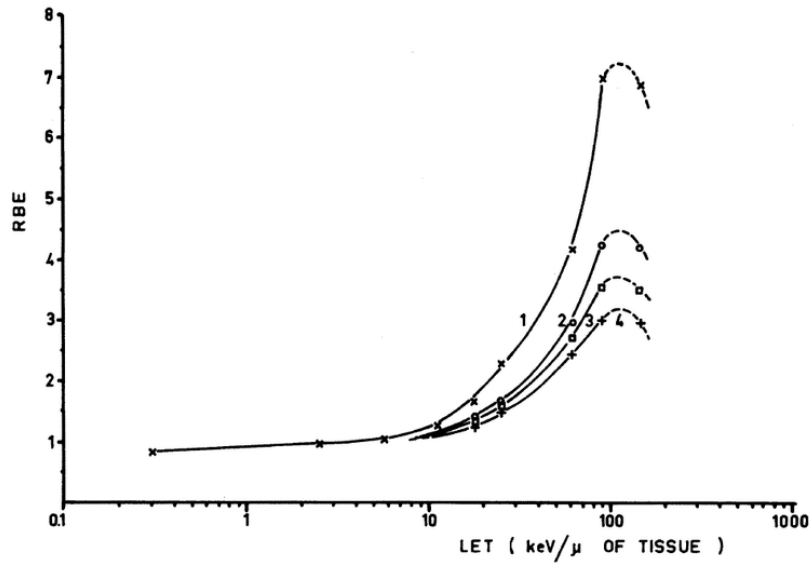


Figure 1.7: The graph shows the relation between the RBE and the LET [11]: RBE increase while LET increase until it reaches the (about)  $100 \text{ keV}/\mu\text{m}$  threshold, in that case despite the high energy deposited, the biological damage always remains the same with a consequent consumption of unnecessary energy, that is why the RBE decreases whilst LET increases. The different curves (1,2,3,4) are related of RBE measurements on different cell survival fractions, as studied in [11].

### 1.3 Monte Carlo codes

The needs of today's physics are connected to the necessity to solve problems that are gradually becoming more complex because the understanding of the reality being studied has become better; today, these answers can be determined by following two distinct paths [12].

The first is to follow a *deterministic approach*: once the problem has been described with correct mathematics and the difficulty of its resolution recognised, one can choose to simplify the actual model with appropriate approximations and find an analytically exact solution for it.

The second is to use the *technique of Monte Carlo calculus*, which allows to determine approximate solutions, through the use of statistics, to exact representations of the models of reality.

Both paths have various advantages and disadvantages but the today's constant development of technology has made it possible to optimise Monte Carlo techniques that have become fundamental and active integral parts of the field of physics research.

In fact, with the Monte Carlo technique, it is possible to simulate the transport of radiation in matter [13] if the cross sections of all the processes involved are

known, using a random number generator.

The idea behind the technique is to be able to exploit the interaction cross-sections as a probability density function of random variables, and thus allow to simulate the path of a particle by taking into account certain fundamental characteristics such as the environment in which it is to be transported and its energy.

Thus, in the case of transporting a particle, the geometry and materials of the simulation environment are known, and the energy of the particle is known, the Monte Carlo acquires the data on the cross-section taking into account the parameters just listed and samples it. Using the random number generator, it can then choose where and when a specific interaction will occur, taking into account the physics of the phenomena due to the chosen cross section.

Monte Carlo codes simulate the *history of a particle*: they follow its path until it disappears, i.e. when it is either absorbed, its kinetic energy becomes zero or when it exits the outside world. The history of a particle also includes any secondary particles that were generated during the history, which are paused during the simulation and simulated as soon as the parent particle is exhausted.

The Monte Carlo method has the disadvantage that it can only simulate one particle at a time, so each one of them is separated in space and time from the others, but its greatest advantage is that it can simulate the statistical behaviour of everyone and then average the results obtained from all the particles simulated.

The value found by the Monte Carlo is the more similar to that expected by the real model, the greater the number of particles it has simulated and, therefore, the greater the sampling it has done.

### The Figure of Merit

Sometimes it is necessary to obtain precise results in a defined time. But *precision* and *timing* are two different operational quantities that both depend on the number of particles simulated, even if in different ways.

The *precision* is a quantity that describes how the results is statistically close to the expected true value and uses the *relative error*  $R$ , related to the result, as a control. The relative error of the average  $m$  of the results of the simulation particles is the ratio between the average variance  $\sigma_m$  and to the value of average, so it is proportional to the square of the number of particles, Eq. ( 1.10). On the other hand, time is proportional to the number of simulated particles in a linear way, Eq. ( 1.11)

$$R = \frac{\sigma_m}{m} \propto \frac{1}{\sqrt{N}}; \quad (1.10)$$

$$t \propto N. \quad (1.11)$$

It is important to note that we can't increase  $R$  or  $t$  separately, but they are connected through  $N$ , so we have to consider this relationship to calculate the best computational time to get a good statistic [12].

For this reason, we could define a parameter called *Figure Of Merit* or *FOM* Eq. ( 1.12) which takes into account the two parameters. *Figure Of Merit* is

defined as [14]

$$FOM = \frac{1}{R^2t}. \quad (1.12)$$

*FOM* is a number that has no unit of measurement: it is a constant and the higher its value is, the better will be the performance of our code, both in terms of time and precision.

### 1.3.1 Condensed History and Truck Structure Codes

Nowadays there are several Monte Carlo codes that follow different approaches taking into account some simulation parameters, such as the quality of the radiation, the size of the target to be studied or the details expected in the outcome [15]. They can be distinguished into two different groups: the **Condensed History**(CH) and the **Truck Structure** (TS) codes.

The CH codes describe the interactions, in the simulation environment, by exploiting the concept of *virtual step*: they follow the track of a particle and define an arbitrary length called *step*, inside which they condense all the interactions that occurred for the single particle and return only the values that the simulation took just before and after the step.

This allows the simulation to speed up, but affects the spatial accuracy of the local energy deposition [16]: this kind of approach can be very useful in experimental studies where it is important to obtain a result on a scale of no less than a millimetre, for example for dosimetry studies on tissues or organs [13].

Nowadays a lot of codes such as EGS, PENELOPE, MCNP and FLUKA can be used for calculating dose in radiotherapy and other medical applications, each one of them is specialised for a specific particle transportation and validated but no one of them have the suitable accuracy to describing physics in the micrometer scale.

In recent years, the demands in the field of radiobiology have instead proposed the development of the Track Structure Codes, that are capable of simulating and recording, step by step, interactions and energy depositions, on the micrometer and nanometer scales, hence the typical dimension of the cells and their compartments.

The main idea in developing track structure codes, in order to satisfy the just showed reached objectives, was to lower the spatial resolution of the Condensed History codes, which depends on the *electron cutoff energy*, by transporting electrons up to an energy equal to the threshold ionisation energy of biological matter (equivalent to water), about  $8 - 10 eV$ .

Some examples of these codes are NOREC, PARTRAC, and KURBUC, more recent developments are enclosed in PENELOPE.

Some of them, as GEANT4 offers also the possibility to both simulate particle transport using a condensed history or a track structure approaches thanks to the recent developments of the GEANT4-DNA.

## 1.4 GEANT4: A brief introduction

GEANT4 was created to respond to the needs of simulating with better accuracy the radiation-matter interaction and to share the outcomes within a wide scientific community. This necessity has led to the founding of two different groups

that later merged into the GEANT4 Collaboration<sup>1</sup> [18] who have combined their knowledge to modify the previous Geant3 code with the goal of improving simulations by incorporating the most modern computing techniques [17] [19]. The toolkit they have developed is called GEANT4 (an acronym for Geometry and Tracking) and they still collaborate today to continuously optimise and expand it.

One of the strengths of GEANT4 is that the code has object-oriented technologies: this allows the user to manage all parts of the toolkit independently marking a big difference to the Geant3 code, written in *FORTRAN* [20] language.

In addition, GEANT4 is an open source toolkit that allows free access to all its developments and to examine and manipulate every component of its source code.

Furthermore, the cross sections can be implemented in various ways but, for those imported from databases, GEANT4 extracts information and uses it in a completely different and separate way, which allows you to implement your own database and fill it with processes and models tailored on parameters such as particle type, energy or materials [17].

In GEANT4 there are keywords that have specific meanings inside the code, different than the typical meaning in common language. These words are called “Primer of terms” [21], some of them are listed below:

- *Track*: instantaneous image of a precise point in a particle path: thanks to this snapshot, the user gets information about particle momentum, energy, position and so on;
- *Trajectory*: a set of snapshots of the same particle;
- *Step*: is the length of two definite points within a particle path. It is chosen by default considering particle physics processes and the simulation detail levels or it can be fixed by the user thanks to the class *G4Step* according to its requests.
- *Event*: an interaction between a primary particle and a target, managed by the class *G4Event*;
- *Run*: a collection of events that can be controlled thanks to the class *G4Run*;
- *Process*: it assumes two different meanings according to the context to which it refers. It is both an application which is being executed and a particle physical interaction;
- *Model*: is a component of a physical process which “can play complementary or alternative roles” [17]. To simulate an interaction, a process may consider several characteristics such as the energy involved and called different models each time, chosen in a way to better describe each of the specific interactions that may occur.

---

<sup>1</sup>is a collective of scientists such as physicists, web developers and engineers from different parts of Europe and the world as Russia, Japan, Canada and the United States [17]

### 1.4.1 Software architecture

GEANT4 is a toolkit composed by free software packages which can be used to accurately simulate the passage of particles through matter [18]. It was written using the C++ [22] language and that place GEANT4 within a perspective of object-oriented technologies: the C++ has made the code easier to implement and has given the users the possibility to better understand links between the different inner structures, giving them the opportunity to manage separately every single code components. A Simple scheme of GEANT4 class categories is illustrated in the Fig. 1.8.

The relations in the diagram 1.8 are unidirectional and the categories at the bottom are connected by those at the top and so are able to use all of the information the latter ones had stored.

Reading from the bottom upwards, the figure shows the category *Globals* which contains references to system of units, constants, numeric and random number handling [17] and it is related to the other categories thanks to *Intercoms*, a linker between the code and the *User Interfaces*. *Material* is another major category where information about characteristics and physical properties of materials used for the simulations are located.

Two branches originate from *Material* and represent strong connections: the first is directed to *Particle* category thanks to which the user has all the instruments to define the specific particles needed, while the second is directed to the *Geometry* one, which contains the necessary to describe the physical space, hence the volume structures, which particles and matter will interact through. These last two categories are connected to *Track* one, where the libraries for constructing the tracking and/or steps can be found.

The *Track* category is then related to *Processes* one where several physical models for each process are available to be chosen.

The description of the evolution of a track is made in *Tracking* category so is easy to understand the connections the category has with the *Event* category, which allows to describe events and with the *Digits+Hits*, that gives information about sensitive volumes already defined.

In addition, the category *Run* takes all of these information, enclose in the categories below it, and manages outcomes required by the simulation.

In the GEANT4 code there is, also, the possibility to activate the graphics representation of simulations using the QT libraries, such as the *OpenOGL* (Open Graphics Library) and, furthermore, to analyze the results directly called the *root* programs and set the format of the output as *.root* file.

### 1.4.2 GEANT4 examples

The GEANT4 Collaborations have included a number of *examples* in the toolkit. These are ready-to-use applications provided with their source code distribution that are useful for simulating common situations and they are easy modifiable to implement one's own projects [15]. The available examples are divided into three categories, depending on the level of complexity and subject matter.

The first category is the *basic examples* and is useful for the understanding of the basic functionality of the code [17] and construct simple applications.

The second is the *extended* category, where users can find a wide domain of applications, such as electromagnetic and hadronic interactions, simulation of

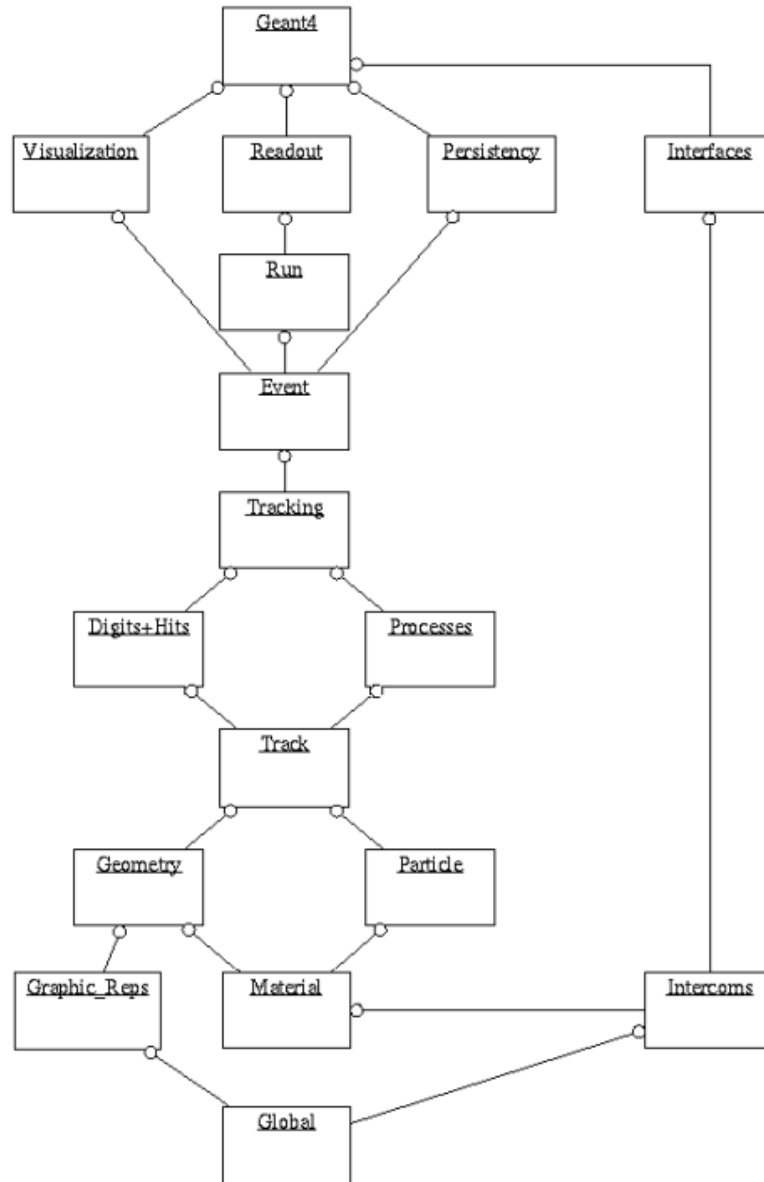


Figure 1.8: GEANT4 class categories. The open circle on the joining lines represents a using relationship; the category at the circle end uses the adjoined category [18]

how to generate histograms with *Root*, radioactive decay resulted from nuclear interactions and much more.

The third is the *advanced* category, comprising complete codes related to nuclear experiments, medical applications and other fields.

### The B1 example and his use for hadrontherapy

The B1 is a basic example mostly used by beginners to learn about the code structures and the links between the fundamental categories.

The B1 example is accessible at a github-repository, available on *gitlab.cern.ch* website [23]. The author, Gabriele Cosmo, also provides a README.txt that contain a list of all the B1-files and a description of their functionality.

There are two folders: the "src" which encloses the code source file and the "include" with the header files.

In the same repository there are also the "main file", a few "macro files" and an output sheet recognizable because of the .out extension.

The source and the header files are both six and they will be better illustrated below.

The first files, the *DetectorConstruction* is about the geometry construction, therefore the definition of materials, volumes and their sensitive parts which will be the detectors. The second is the *ParticleGeneratorAction* in which the mandatory class of *ParticleGenerator* is instantiated to consent the definition of the particle source and its characteristic as energy, momentum, space position and direction. The third, the fourth and the fifth are connected: they are called *SteppingAction*, *EventAction* and *RunAction* and, in there, are implemented the Action Classes useful to simulate the steps, the events and the run of the simulation. The B1 example, in particular, describes the detectors response to energy deposition; the depth dose profile is calculated thanks a function called *Geant4AccumulableManager*.

Instead, the Physics list used is the **QBBC**, an internal GEANT4 nomenclature for library, which encloses the QGSC, Bertini, BinaryCascade and CHIPS physics [24] [25], for the description of high energy physics. The implementation is set directly in the main file, there's not a source file dedicated to it (as it happens in all of the others GEANT4 examples): the appropriate processes and models are just selected by default according to the users requests, during the simulations.

The last, the sixth file, is called *ActionInitialization* and here are instantiated and registered, to the GEANT4 kernel, all user action classes.

B1 example was adapted to calculate the protons energy deposit and the characteristic dose profile in water for a protons pencil beam, for medical application in hadrontherapy.

The geometry was simplified with a cylinder with a 6 cm of diameter, made of water, oriented along z-axis, 30 cm high, encapsulated into a 20x20x30 cm air box, as shown in the picture Fig. 1.9 on the left.

The source was pointwise and the particle type was 100 MeV protons, shot along to the water cylinder, i.e., along z-axis.

The connection between steps, events and run were not modified but the outcome was obtained by the use of a *Mesh*, written in a macro file. The box and the cylinder were divided into 3 thousand, 0.01 mm thick consequent layers,

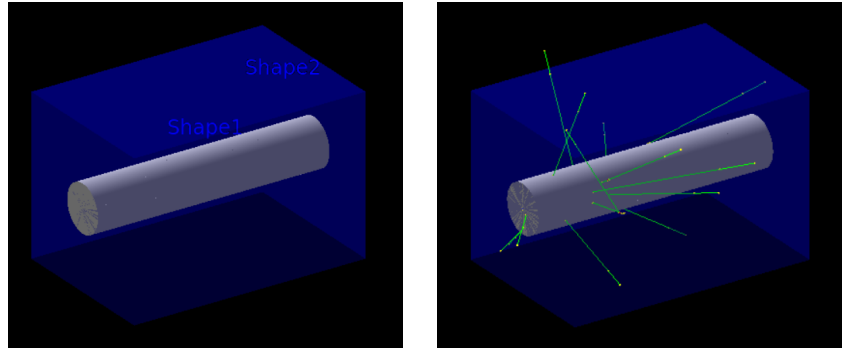


Figure 1.9: Left: the new Geometry implemented in B1 example and visualized with OPENGL: there are the box, in blue, and the cylinder made of water, in white. Right: simulation of a proton beam of 100 particles with 100 MeV energy through the same geometry, visualized with OPENGL in GEANT4. Tracks in different colors describe several particles: photons in green, electrons in red, protons in yellow. Yellow points represent general points of interactions.

protons were generated directly in the top of the sensitive volume, the cylinder, straight along its axis. An example of proton beam simulation is shown in the right panel of Fig. 1.9.

Once compiled the macro file with the instruction to construct and execute a mesh and running it coupled with the example, it is possible to visualize how protons have penetrated the cylinder for about 8 cm, according to their energy. The output is stored in a text file, which can be read within a *Jupyter Notebook* [26], with a python environment containing NumPy and Matplotlib [27, 28]: in this set-up we were able to reproduce the dose-depth profile, i.e. the characteristic Bragg Peak Fig. 1.10.

## 1.5 GEANT4-DNA: the GEANT4 extension to simulate DNA damages

One of the requirements in biomedical physics is to know more about the effects of ionizing radiation interactions with biological system. In order to improve the modelling capability of simulators, researchers need more experimental data for validating the simulation results.

While high-energy particles interaction with biological matter was well characterized, especially from the Nagasaki and Hiroshima bomb disaster [29], it was clear that dose-effect relationship due to low-energy radiation needed more investigation.

In 2001, an idea by P. Niemen responded to the European Space Agency necessity for having a software capable of simulating DNA damage for future astronauts who might be involved in solar particle events or exposed to cosmic rays [29]. The choice was to extend the part of the GEANT4 toolkit to the low energy domain (down to the eV scale) [30], investing into an open source development.

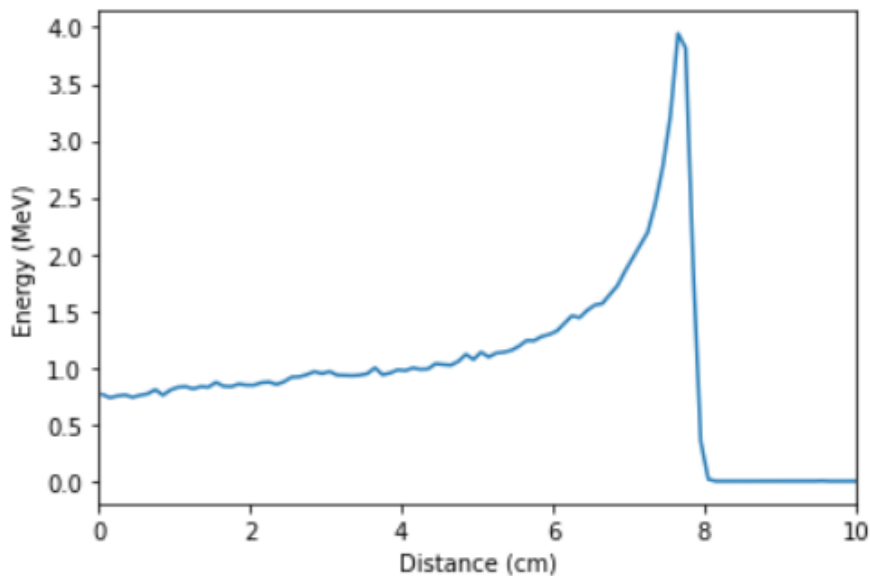


Figure 1.10: Proton Bragg Peak. The chart, made with *Jupiter Notebook*, shows the outcome of a simulation of 10 thousand protons of 100 MeV energy. X-axis represents the depth in water in *cm* and y-axis, the energy in MeV.

As a result, in 2007, the extension of the toolkit was published and first released under the name GEANT4-DNA. A GEANT4-DNA Collaboration was formed by the GEANT4 Low Energy Electromagnetic Physics Working Group of the GEANT4 collaboration [29], which today continues to improve the functionality of the extension.

GEANT4-DNA package uses a Monte Carlo approach, because "the physical, chemical and biological interactions of radiation within an organic medium are stochastic processes" [31]. However GEANT4 is a condensed history code and, how it was saying in paragraph 1.3.1, it implies that the results obtained is lacking in precision in the descriptions of the consequences of irradiation at the nanoscale [31], essentials for predicting the biological damages at DNA scale. GEANT4-DNA thus adopted a track structure approach: it simulates step-by-step interactions of a single particle, also following secondary electrons down to the excitation or ionization threshold of the medium, (in the 7–10eV range for liquid water) [15].

Today the toolkit extension is able to simulate the path of single particles (such as electrons, protons and neutral hydrogen atoms, alpha particles including their charge states, and a few ions – Li, Be, B, C, N, O, Si, Fe) following them in their step-by-step interactions with liquid water and with the DNA constituent as Adenine, Thymine, Guanine, Cytosine, and backbone [15]. What makes GEANT4-DNA a powerful tool for radiobiological studies is its ability to simulate the physico-chemical and chemical phases of water radiolysis in the irradiated medium down to 1  $\mu$ s after irradiation. Profiting from GEANT4

capabilities, this code allows to model the geometry of different biological targets in the micrometer and even in the nanometer scale.

### 1.5.1 Key package features

GEANT4-DNA has at its disposal, as in GEANT4, a number of objects for describing real physical processes involving different types of cross sections, such as those for inelastic and elastic scattering, excitation, ionisation and more.

A process permits a complete description of the products of the interactions, for example the secondary particles, the kinematics or the energy deposition. Each process is located within a *class of processes*, also written in C++, which is identified by the tag *G4DNA $XXX$*  where *XXX* is the name of the process the user intends to use.

The physical quantities to be calculated are obtained by the use of specific models. Many models, grouped in a *class of models*, can be involved in a single process. They are distinguishable from processes by a different tag *G4DNA $YYYXXXModel$*  where *YYY* denotes the name of the model and *XXX* relates to the name of the process: it is impossible to use a model without first declaring the physical process involved in the simulation.

All the processes and the models in GEANT4-DNA have been validated using reference data from NIST<sup>2</sup> or ICRU<sup>3</sup> and experimental data *wherever available*, or other Monte Carlo codes simulations [15].

GEANT4-DNA collaboration has built some specific objects called *constructors* which generally contain processes for calculating specific physical interactions and also some models to calculate the main physical quantities, the most required ones, connected with the simulated processes. In about 10 years, many constructors have been published in the official GEANT4-DNA repository since GEANT4 10.4 releases [15]. Later, chemical constructors have been implemented as well.

Fig. 1.11 reports three of the most used constructors for simulating electrons track in liquid water, with processes and models comprised. It is interesting to note how they differ mostly in the physics used for simulate electrons interactions: this determine a remarkable differences between each one of them and forces to selected them just in function of the best response in electrons simulations based on low, medium or high energy involved.

### 1.5.2 How to model a track structure

Biological tissues are mostly composed of liquid water: when radiation interacts with them, it might caused ionization and excitation in water molecules, that generally dissociate due to a set of virtually instantaneous reactions depending on the radiation energy deposition [34].

The dissociation products of water are a hydronium  $H_3O^+$  and a hydroxyl  $OH^-$  radical, generally responsible of indirect damages to the DNA molecules.

The real amount of damages for biological systems are only detectable after hours or sometimes longer time, even years, so the use of a software to predict

<sup>2</sup>National Institute of Standards and Technology - NIST [32]

<sup>3</sup>International Committee for Radiological Units [33]

## 1.5. GEANT4-DNA: THE GEANT4 EXTENSION TO SIMULATE DNA DAMAGES<sup>29</sup>

Geant4-DNA physics constructors electron models			
Process	G4EmDNAPhysics_option2	G4EmDNAPhysics_option4	G4EmDNAPhysics_option6
Ionization (inelastic)	Emfietzoglou dielectric model (11 eV–1 MeV) <sup>5</sup>	Emfietzoglou–Kyriakou dielectric model (10 eV–10 keV) <sup>47</sup>	Relativistic binary encounter Bethe model from CPA100 code (11 eV–256 keV) <sup>48</sup>
Electronic excitation (inelastic)	Emfietzoglou dielectric model (9 eV–1 MeV) <sup>5</sup>	Emfietzoglou–Kyriakou dielectric model (8 eV–10 keV) <sup>47</sup>	Dielectric model from CPA100 code (11 eV–256 keV) <sup>48</sup>
Elastic scattering (elastic)	Partial wave model (7.4 eV–1 MeV) <sup>5</sup>	Uehara screened Rutherford model (9 eV–10 keV) <sup>47</sup>	Independent Atom Method model from CPA100 code (11 eV–256 keV) <sup>48</sup>
Vibrational excitation (inelastic subexcitation)	Sanche data (2 eV–100 eV) <sup>49</sup>	n/a	n/a
Attachment (inelastic subexcitation)	Melton data (4 eV–13 eV) <sup>50</sup>	n/a	n/a
Auger electron emission	From the EADL database <sup>51</sup> and the Geant4 atomic relaxation interface <sup>52,53</sup>		
Default tracking cut <sup>(*)</sup>	7.4 eV	10 eV	11 eV

Figure 1.11: The list shows the processes and models placed in *G4EmDNAPhysics – option2*, *G4EmDNAPhysics – option4* and *G4EmDNAPhysics – option6* with their energy range of applicability. The (\*) indicates that, below the threshold, the energy of particles are locally deposited [15].

the behaviour of irradiated cells, requires a deep understanding of biological and physical laws that govern the living systems.

Next paragraphs describe in more details the GEANT4-DNA simulation of the stages of radiation interactions that were represented above in Fig. 1.5 and separately implemented therein.

### Physical stage

The simulation of the physics stage describes all the electromagnetic interaction of radiation in matter, thanks to availability to have information about the interaction probability of all the primary and secondary particles produced [35]. To date, experimental data describing the ionization and excitation cross sections in liquid water are not available, however experimental data on gaseous water (vapor) do exist. For this reason, the developers used data from spectroscopy which provides the absorption spectrum and the optical dielectric constants for liquid water, from which the inelastic scattering cross sections are indirectly derived [16].

GEANT4-DNA project framework includes theoretical models providing different ways of calculating cross sections and gives the user the possibility to chose the most suitable according to the specific simulation. For example, a model could be preferred because of its optimized description in a given energy range.

### Physico-chemical stage

This stage describes the electrons thermalization process: ionizing radiations deposits energy in the matter, thorough ionization and excitation of electrons presents in water molecules which begin to move and transfer energy (secondary electrons).

In GEANT4-DNA five dissociation channels are available to simulate the processes according to the energy involved: they are show in Fig. 1.12 along with their branching ratio.

Electronic State	Decay Channel	Fraction
All ionization states	$\text{H}_2\text{O}^+ + \text{H}_2\text{O} \rightarrow \text{H}_3\text{O}^+ + \bullet\text{OH}$ (through proton transfer)	100%
Excitation state A1B1: (1b1) $\rightarrow$ (4a1/3s)	$\text{H}_2\text{O}^* \rightarrow \bullet\text{OH} + \text{H}\bullet$	65%
	$\text{H}_2\text{O}^* \rightarrow \text{H}_2\text{O} + \Delta\text{E}$	35%
Excitation state B1A1: (3a1) $\rightarrow$ (4a1/3s)	$\text{H}_2\text{O}^* \rightarrow \text{HO}^+ + \bullet\text{OH} + \text{e}^-_{\text{aq}}$	55%
	$\text{H}_2\text{O}^* \rightarrow \bullet\text{OH} + \bullet\text{OH} + \text{H}_2$	15%
	$\text{H}_2\text{O}^* \rightarrow \text{H}_2\text{O} + \Delta\text{E}$	30%
Excitation state: Rydberg, diffusion bands	$\text{H}_2\text{O}^* \rightarrow \text{HO}^+ + \bullet\text{OH} + \text{e}^-_{\text{aq}}$	50%
	$\text{H}_2\text{O}^* \rightarrow \text{H}_2\text{O} + \Delta\text{E}$	50%
Electron attachment	$\text{H}_2\text{O}^- \rightarrow \text{OH}^- + \bullet\text{OH} + \text{H}_2$	100
Electron-hole recombination	$\text{H}_2\text{O}^* \rightarrow \bullet\text{OH} + \text{H}\bullet$	55%
	$\text{H}_2\text{O}^* \rightarrow \text{H}_2 + 2\bullet\text{OH}$	15%
	$\text{H}_2\text{O}^* \rightarrow \text{H}_2\text{O} + \Delta\text{E}$	30%

Figure 1.12: The five dissociation channels implemented in the toolkit, to simulate water molecules dissociation until  $1ps$ , the symbol "\*" represents the excited water molecules, more details in [16]

### Chemical stage

Simultaneously the Physico-Chemical processes, from  $1ps$  up to  $1\mu s$  the Chemical stage starts and the reactive chemical species produced by the dissociation of water molecules begin to diffuse and interact with the biological structures. The diffusion process is described by the Brownian equation which is the solution of the Smoluchowski equation [16]

$$p(r, \Delta t | r_0) = \frac{4\pi(r - r_0)^2}{(4\pi D \Delta t)^{3/2}} e^{-\frac{(r-r_0)^2}{4D\Delta t}} \quad (1.13)$$

where  $p$  is the probability that in a time  $\Delta t$  a species can reach the position  $r$  from  $r_0$ .

This function can be applied in a 3D reference system on the  $xyz$  - axes or in a *polar* one and a random generator is used to calculate the time dependent random position where an interaction may occur. Furthermore, this result is strictly dependent on the diffusion coefficient  $D$  and the water, the medium in which the reactants are found, is represented as a continuum.

With this theory is possible to define a reactant coefficient  $k$ : its value is determined according to the different probability of each molecule to form a complex, dissociating or activating, and depends on a certain proximity threshold.

In the case of uncharged particles, it is defined as

$$k = 4\pi N_A D \quad (1.14)$$

and for electrostatic interactions, the Smoluchowski-Debye theory find  $k$  as

$$k = 4\pi N_A D \sigma_{eff} \quad (1.15)$$

where  $\sigma_{eff}$  is a function that depends on Onsager distance and the reaction radius,  $N_A$  is the Avogadro number,  $D$  the diffusion coefficient (more details

can be found in [16]).

Since these simulations are time-consuming and require substantial computational resources, all the diffusion processes were before simulated by using small step [36]. But, to not overlook possible reactions that might occur along the path of a particle, time interval of species in diffusion can't be too small [37] hence an improvement of the time step concept was implemented as a strategy to optimise these calculations.

The Step by Step, *SBS*, approach use the dynamic step model, calculating with the equation 1.13, and defines a virtual time step during which reactions between reactants can take place with a confidence level of at least 95% [16]: i.e. a particle can be considered "free" during its path.

Steps have to be simulated until a chemical interaction occurs, that it means that sometimes a lot of steps are collected but in this way is prevented any loss of information.

The user can also decide to set in on code, modifying the number of steps using two different approaches called the Brownian Bridge and the Minimum Time Steps which are implemented in chemical constructor G4EmDNAChemistry and G4EmDNAChemistry-option1 and available to be used.

### 1.5.3 The Geometry in GEANT4-DNA

With the aim of simulating and predicting DNA damages due to radiation interactions, the users can follow three different approaches: the first is to use a cluster algorithm to obtain an estimate of DNA damages, the second is to make a simulation of irradiation through biological targets already implemented in GEANT4 geometry and the third is a mix of the previous two [31]. A brief description is given below.

#### A cluster algorithm

As anticipated in Section 1.2.3, a single track can lead to the formation of SSBs or, if there are more than two SSBs in less than ten bps, a DSB. Additionally, if within these ten bps, the DNA molecule has been damaged by more than one DSB, this is referred to as a cluster of damages. For example, a cluster is usually caused by high LET particle irradiation.

A cluster algorithm is an algorithm in which the simulation of DNA damages consists of studying the pattern of energy deposition by ionizing radiation [31]. The pioneers were Francis et al. [38] who realized their own code on an adaptation of the DBSCAN algorithm [39]. Unfortunately their code was not available for *GEANT4* users; some times later, the Perrot's group [35] realized a similar study now published in *GEANT4 "extended/medical/dna"* repository under the example name "clustering".

The main idea was to give users the possibility to first define their own meaning of cluster, taking into account the concept of *proximity of damages* (SSB or DSB) and to set parameters such as the "minimum number of interaction points to form a cluster, the probability that a point falls within a sensitive region of a target, the maximum distance separating two points in a cluster and the probability to induce a strand break [31]". Subsequently, the user manages these parameters during the simulation, and modifies them thanks to the

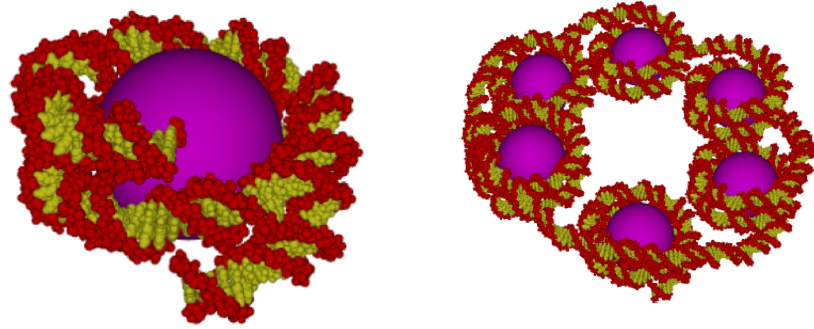


Figure 1.13: Representation of a nucleosome, on the left, and a chromatin fiber of 30 nm, on the right, of the B-DNA molecule [35]

specific category in the GEANT4 visualisation user interface. Then, once the definition is set, the code of Perrot et al. is ready to find all the clusters produced by the irradiation of the DNA molecule and finally it provides the user the outcome of the irradiation. An example of this approach can be found in the study published by Bernal et al. in 2015 [35] where the group simulated the modelling of trace structure in liquid water.

GEANT4-DNA packages also benefit from the geometry implemented in GEANT4 and thus from all the developments the code has had and continues to have.

### Implementing geometry

A way to simulate radiation-matter interaction is thus to first implement GEANT4 geometry to model the biological target such as the entire DNA molecule, the nucleosome or nitrogenous bases, and then start simulating the physical, physico-chemical and chemical phases of radiation interaction.

Modelling the DNA double helix and associated biological structures of interest can be realized with an Atomistic approach or a Voxel approach.

In the Atomistic approach all the structures are constructed approximating the biological volumes by simple mathematical geometry shapes such as spheres, cubes or cylinders. This provides a simplified representation of the biological compartments that would be really difficult to reproduce in their real geometrical composition.

Examples of this are the B-DNA construct (Fig. 1.13) by Bernal [40], the simplified nucleus made of randomly oriented short segments of chromatin fibres, for a total of  $6 * 10^9$  bp. [31] defined by Incerti et al. [41] and the simulation of Samsra et al., including a representation of the DNA chain encapsulated inside a water cylinder to better simulate indirect damages, inspired by Pollon's work.

Today users can find a GEANT4-DNA example called whole-nuclear-DNA, consisting in the description of a fibroblast cell nucleus with the DNA molecule and her nitrogenous bases, phosphate groups and other special structures in five different organization levels ( Fig. 1.14). With this example it is possible to simulate direct and indirect damages [42].

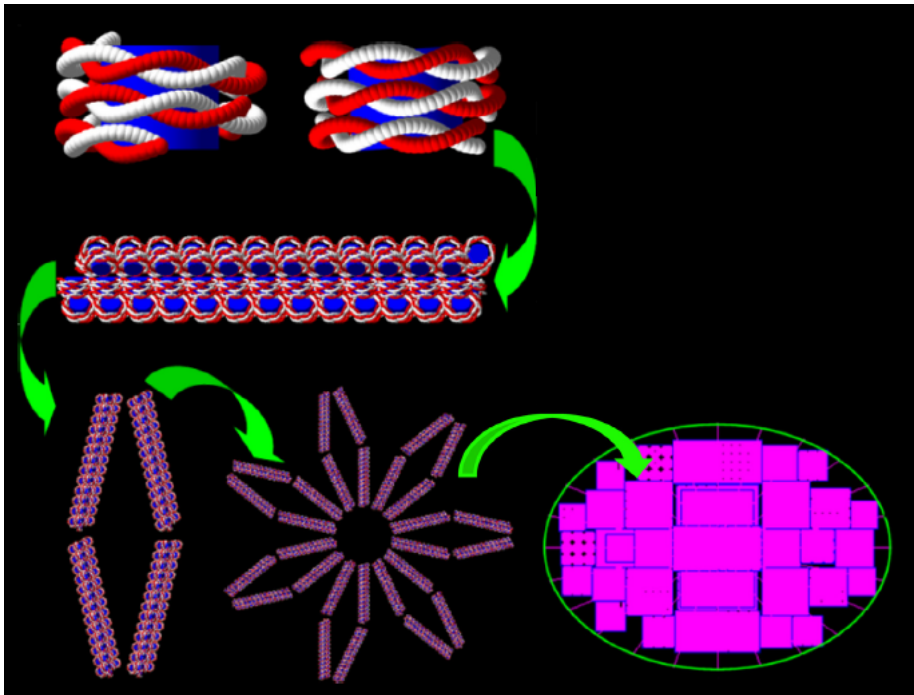


Figure 1.14: Representation of the five organization levels of a DNA molecule inserted into fibroblast cell nucleus, implemented in WholeNuclearDNA example. The cell nucleus contains the  $6 * 10^9$  base pairs. Top: two figures of DNA double helix, Middle: the nucleosome, and Bottom: the chromatin fiber: 90 nucleosomes arranged in an helix, “flower” loops consisting of 28 chromatin fibers, chromosome territories [42].

Even though this representation returns to users a full description, it is sometimes useful to increase the precision of the description of biological volumes, so there is a second approach in which the granularity of DNA molecule has been improved, using information from real CT scans of patients.

This approach is called Voxel approach, and makes it possible to study what happens when radiation crosses each voxel of the geometry. A demonstration of it was provided in “pbdna” example [43], where the authors used the data from the “Protein Data Bank” in order to have a more specific representation of a real DNA molecule. The example is already available and placed in the same GEANT4 repository “extendend/medical/dna”; the outcome of two different simulations is shown in Fig. 1.15.

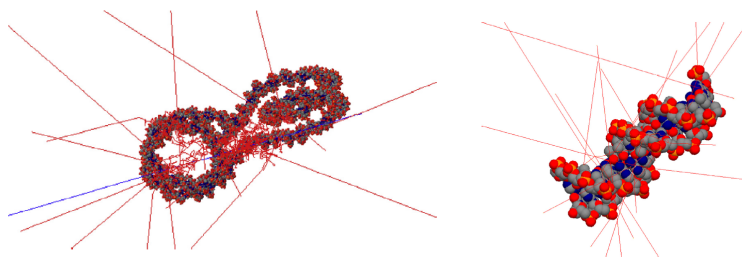


Figure 1.15: Left: rendering of the atomistic view of a dinucleosome irradiated by a single 100 keV proton using the “extended/medical/dna/pdb4dna” GEANT4-DNA example. Taken from [35]. Right: Example of irradiation of the 3BSE 16-base-pair B-DNA PDB molecule by 10 incident 10 keV electrons, simulated with the GEANT4-DNA “pdb4dna” example. Taken from [31].

1.5. *GEANT4-DNA: THE GEANT4 EXTENSION TO SIMULATE DNA DAMAGES* 35

# Chapter 2

## Materials and methods

### 2.1 The experimental configuration

In this chapter the equipment and set up used for studying biological damages induced by photon irradiation on cells will be described.

The experimental set-up is located at the Biophysics Laboratory of the University of Naples and measurements were carried out in July 2022.

#### 2.1.1 The X-ray Tube

The X-ray tube used for the irradiation is a diagnostic apparatus, a *STABILIPAN 2* machine manufactured by Siemens in Munich (Germany) nowadays only dedicated to didactic and research experiments. Fig. 2.1 shows a picture of the instrument.

The production of X-rays is obtained thanks to the presence of a Thomson tube (TR300F) equipped with a tungsten anode, with a 30 degree inclination, at  $250kVp$ , and filtered by 1-mm-thick Cu foil.

The photons produced by electron interaction in target, can escape only passing through a Plexiglass window provided with a 1 mm thick Cu filter.

The white box under the filter visible in Fig. 2.1 encloses some optical shutters not influencing the samples of the measurements described in this thesis. For this reason, in the Geant4 simulations it has been not described in detail.

The table 2.1.1 lists the X-ray STABILIPAN tube characteristics.

Voltage	Anode	Anode inclination	Filter
$250kVp$	Tungsten	$30degrees$	$1mmCu$

#### 2.1.2 The experimental set up

The Petri Dish in 2.1 contains the cells selected for the experiment, specifically the UMR106 cell line, an epithelial-like cells isolated from the bone of a rat suffering from osteosarcoma [2]. This cell line has been selected because they have been object of extensive BNCT research at the University of Pavia [3].

The cells were first treated following a precise protocol, reported in appendix.

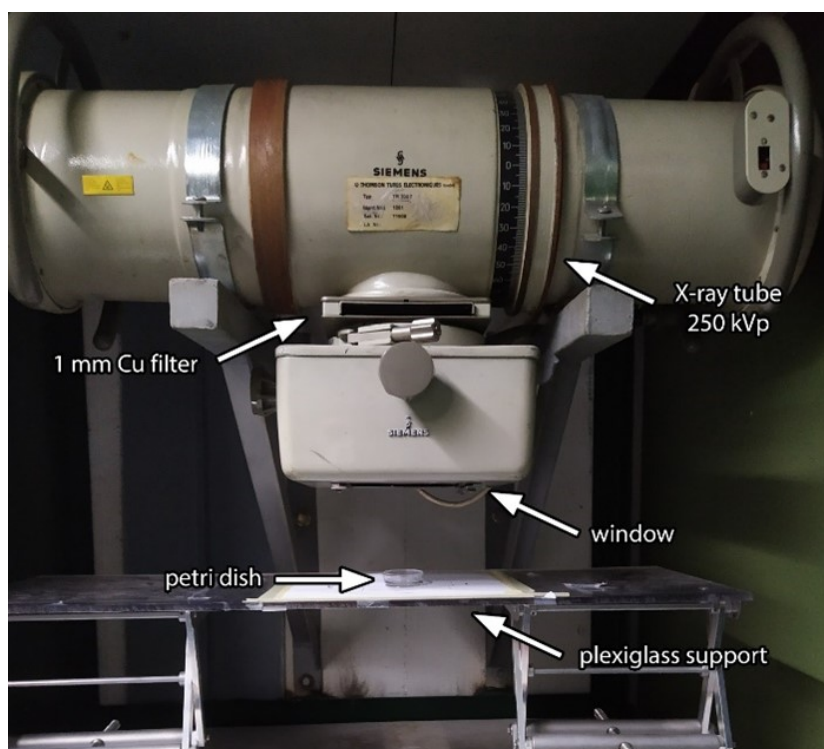


Figure 2.1: The X-ray Tube by STABILIPAN at the Biophysics Laboratory of the University of Naples and the experimental configuration adopted, July 2022.

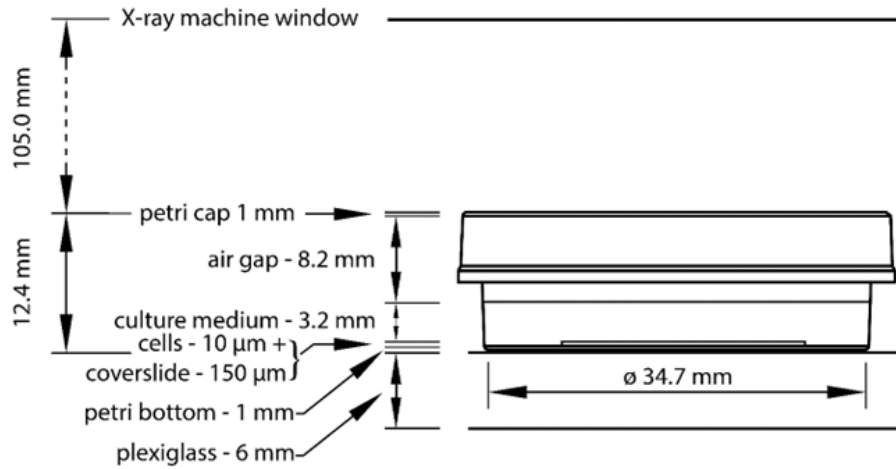


Figure 2.2: Scheme describing the experimental set-up of cells inside the petri dish.

For the irradiation, they were seeded on  $24 \times 24 \text{ mm}^2$  borosilicate glass coverslips, which were in turn placed inside petri dishes of  $35 \text{ mm}$  of diameter (Falcon<sup>®</sup>), made of polystyrene (PS)), and positioned on a plexiglass table equipped with handles to adjust its height.

Photons emerging from the window above go straight to the petri dish; it is assumed that the irradiation is uniform within the cell sample. The cells absorb a dose value which depends also on the several materials interposed between the window and the culture. In details, the cell monolayer is covered by their culture medium (DMEM), a layer of air and 1 mm-thick plexiglass top of the petri dish. This configuration is sketched in Fig. 2.2, highlighting the volume of the medium culture (DMEM) compared to the monolayer of cells, the air gap and the two layers of plexiglas placed at the top and at the bottom of the petri dish.

### 2.1.3 The RADCAL Camera

The calibration to establish the dose to be delivered to cells was obtained by measurement with an ionization chamber. For this experiment, was used the RADCAL AccuPro Ionization chamber [44], model (10X6-06) (Fig. 2.3): it enclose a sensitive volume which is the particle detector and take into account the energy deposit in it, by photon irradiation, at a given energy.

Given this calibration, it is fundamental to place the cell monolayer at the same height of the sensitive volume of the RADCAL chamber, which requires to adjust the table handles  $1.2 \text{ cm}$  lower. At the height fixed, the dose rate measured by the chamber is  $1.37 \text{ Gy/min}$ .

### 2.1.4 The experimental data

The table 2.1.4 reports the irradiation time and the corresponding dose deposit in cells due to the irradiation carried out. Absorbed dose reported were obtained

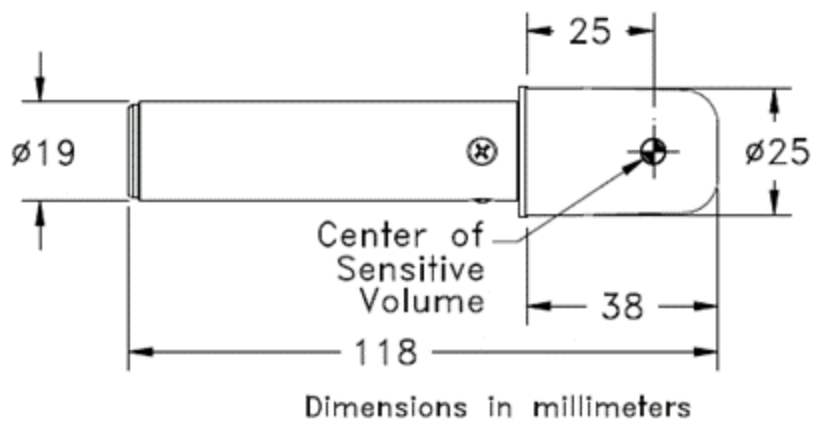


Figure 2.3: RADCAL Ionization Chamber. Top: scheme of the internal structure and its sensitive volume. Bottom: picture of the chamber [44].

based on the calibration described above. One of the goals of this work was to simulate this set-up to verify that the absorbed dose was well calculated with the calibration. This topic will be discussed in chapter 3.

Dose (Gy)	Time (s)
0.5	22
2	88

## 2.2 Simulation of the photon energy spectrum

One of the most important and necessary information for simulating DNA damages in UMR106 cells is the photon energy spectrum.

In order to verify that the dose deposit in the RADCAL chamber was effective the one the cells received, a detailed simulation of the set-up has been carried out. The photon energy spectrum was reproduced using a Python library called **xpecgen** [45] [46]

This library can simulate the impact of an electron beam through an anode and generate Bremsstrahlung and characteristic X-ray emission. The **xpecgen** is user-friendly: by activating the packages, a graphic interface allows modifying certain physical and numerical parameters such as the material and the inclination of the anode or the energy of the electrons, before starting the simulation. It is also possible to decide the number of bins for constructing an histogram and the minimum photon energy threshold. the Analyze window provides a path to add some filters by choosing between different thickness values and several materials.

The data collected as the output of the simulation were stored in *.txt* files that can be analyzed and plotted using an external code.

For this experiment, the data available and reported in tab. 2.1.1 have been plotted in Fig. 2.4

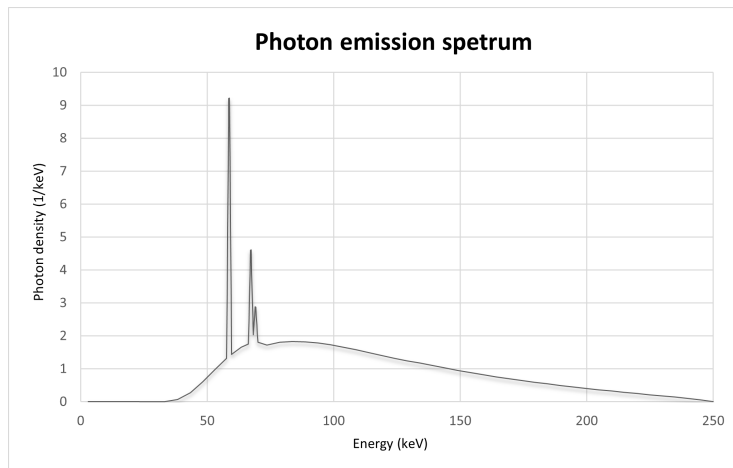


Figure 2.4: The photon energy spectrum generated thanks the xpecgen library, using W anode and 1mm Cu filter.

## 2.3 The available class for Geant4 XRayTube code development

Considering the xpecgen spectrum described above as the benchmark of our simulation, we then simulated it by GEANT4. This step is crucial: it allows obtaining the simulation of the radiation source to calculate the dose absorbed by cells and the interaction of radiation with DNA. It is thus very important that GEANT4 source simulation is well validated against the xpecgen results. To do this, it was first necessary to simulate the set up of Fig. 2.1, to implement the Physical processes involved in this experiment and to construct the electron source as detailed in the following sections.

### 2.3.1 The Geometry

The configuration of the irradiation geometry was set up using the pure virtual Geant4 class **G4VUserDetectorConstruction** [47], which must be implemented before the code is executed, in fact, it cannot be changed during the run.

This class allows representing the geometry with three different levels of description, that depend on specific other related classes:

- *The solid description* is useful for defining the shapes of the geometry, such as boxes, cylinders or other more complex objects.
- *The logical description* associates the volumes created with their main characteristics, for example the material and any magnetic field possibly present.
- *The placement* of the geometry in space: it is possible to use a class called **G4PVPlacement** and to define a position inside the simulation *World*, which is always necessary. It has precise boundaries and contains all the simulated volumes.

In the G4PVPlacement class, the relationships between the shapes just defined and all the volumes placed in the world must be declared. The definition of these hierarchical relations makes it possible to simplify the positioning of the geometry and to build a framework for all the physical processes and particle simulations. These take into account the different materials and world boundaries during the Run.

In addition, in GEANT4, the whole geometry is placed along the Z-axis so there is a method called **G4RotationMatrix**, which can be called in the G4PVPlacement, that rotates the volumes.

### 2.3.2 The Physics List

The physical list is one of the three mandatory parts that must be implemented in Geant4 to start a simulation. Our class and its variables were set up by deriving them from the pure virtual class **G4VModularPhysicsList** [47].

The class is part of the initialisation classes, so it can only be invoked at the start of execution and cannot be changed during the run of the simulation.

To construct the physics of the simulation, two **G4VModularPhysicsList** functions were implemented: *ConstructParticles* to define all the particles to be transported and *ConstructProcesses* to instantiate all the processes and models required for the interactions.

To adopt the correct cross sections to be sampled during the simulation, it was important to include all the libraries of the physics: the main objective was to simulate the transport of electrons and photons and a good choice was represented by the Electromagnetic Constructor called **G4EmStandardPhysics-option4**.

This constructor was selected because today it represents one of the most accurate at low energies: it sets the processes that best describe the behaviour of the electrons as a function of their energy and it activates the models for their interactions (for example in the electron-tungsten interaction, Bremsstrahlung or Characteristic X-ray emission are activated).

In addition, the constructor allows adjusting and setting the right physics for the transport of secondaries particle, such as photons, once the electrons had disappeared.

Other available constructors were implemented in the simulation; they can be called thanks the inclusion of a *messenger list* which directly communicates with the code main and to allow modifying the constructor selected or the processes applied without modifying the code. The messenger list derives its variables and methods from the class **G4UIMessenger** and allows managing this part of the code directly from the graphic interface.

### 2.3.3 The Source

The particle source was set, like the geometry, using another pure virtual class called **G4VUserPrimaryGeneratorAction** [47]: it can be modified after the initialization of the simulation environment because it is part of the Action Classes, which are invoked during the execution of the run, at the end of each event.

This class has methods to place the particle source inside the World of the geometry. For the code XrayTube, the source particles were electrons, sampled inside the inner cylinder that makes up the X-ray tube geometry. The energy of electrons was 250 keV and they had a momentum direction of 1,0,0 (along the x-axis of the inner cylinder). Each electron is generated separately, using a random number generator (**G4UniformRand**), emitting from a surface of 1  $cm^2$  area.

### 2.3.4 The Scoring

The Geant4 toolkit does not save automatically the response of a simulation: at the end of each event, parameters characterising the past interaction are deleted and the result of the entire Run could be lost if not specifically requested. This saves a great amount of memory, however sometimes it is necessary to save not only the final results of the Run but also the outcomes produced after every single particle step.

A solution is represented by the call of specific classes: the **G4ScoringManager**,

### 2.3. THE AVAILABLE CLASS FOR GEANT4 XRAYTUBE CODE DEVELOPMENT<sup>43</sup>

useful for portioning a volume and doing a Mesh <sup>1</sup>, or the **G4VAnalysisManager** to store the results in different format as *Root*, *csv* o *xml*. With these scoring options, it is then possible to save the values and to perform the analysis for example by building histograms by instantiating the *AnalysisManager*, that exploits the C++ technologies to open, write, save and close a file.

For the XrayTube code, the best choice was represented by saving information in a *.csv* extension: in Chapter 3 this part will be discussed.

---

<sup>1</sup>a Mesh is a function that allows reproducing a fictitious sensitive area placed below a specific part of geometry, in which the quantities of interested must be scored

# Chapter 3

## Results

This chapter presents the results obtained from the XRayTube code. The paragraphs are organised as follows: first, the approximations that were necessary to develop the geometry and the particle source are presented, then the tests performed to evaluate the reliability of the code are described and, finally, results are analysed.

To realise the irradiation simulation, it has been necessary to make some approximations: the information used for modelling the experimental set up have been taken from the official manual, stored in the University of Naples, that I personally consulted in November 2022. Moreover, I used the paper [48] reporting figures of the internal structures of the STABILIPAN TRF300X adapted to their medical, Fig. 3.1

### 3.1 Geometry construction and approximations

The first objective to achieve was to realise a reliable set-up of volumes which must ensure a good description of the real machine. It must be considered that the amount of details of the STABILIPAN TRF300 X-ray tube structure is huge and not all of them contribute to the results of the simulations. We thus decided to select and represent only the parts involved directly or indirectly in the irradiation and omitting certain construction components that would not have contributed to the final results.

#### The X-ray tube

The X-ray tube container was modelled by defining two coaxial cylinders of different sizes, the outer,  $3\text{ mm}$  thick, made of lead, and the inner,  $1\text{ mm}$  thick, made of air. Placed inside the container, the X-ray Tube was constructed by defining another coaxial cylinder to the structure, made of Pyrex and filled by the material *Galactic*, called by the NIST library, which is not a perfect void, impossible to insert in GEANT4.

The Pyrex cylinder encloses a tungsten anode, which was simulated with a 30-degree inclination with respect to the axis of the tube, a sketch of the geometry was reported in figure Fig. 3.5 and the simulated one is instead in Figures 3.6

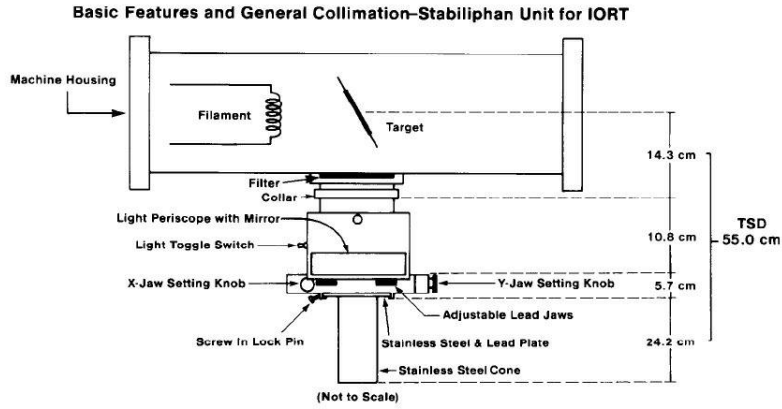


Fig. 5.

Figure 3.1: Scheme of STAILIPAN TRF300 X-ray Tube adapted for intraoperative radiation therapy.

and 3.2

The particles generated by the source located into the X-ray tube, can only escape from a window air, communicating with the structures below, that has been defined cutting the X-ray Tube container using the class **G4SubtractionSolid**. Below the window, the structure is simulated approximating the real one, using two other coaxial cylinders, placed along the z-axis: the first is made up of air and directly communicating with the window just described, the second is made up of lead, providing a shield for the possible outgoing radiation.

Particles are forced to walk through the cylinder and, during their path, filtered with a  $1\text{ mm}$  thick copper disc that prevents secondaries (and possibly particles from source) from passing through if their energy is below a definite threshold. This approximation was considered the best way to omit the presence of the metallic drawer present in the real machine. The copper filter is placed within the drawer, however it is transparent to photons or other particles that cross it and interact only with the copper filter or the structures wall to continue their path.

The last part of the geometry simulates the box showed in the Fig. 2.1: in the XrayTube simulation code, it only has the passive role of directioning the particle beam. In the real one, the machine allow the opportunity to activate optical shutters. According to the objectives of this research, the shutters were not used during this experimental irradiation then, in our simulation, they were omitted. For this reason the box was constructed by defining a plastic material with composition  $C_8H_8$ , filled only with air and covered by a box of lead to rectify a possible loss of radiation. Particles enter inside this box through an air window defined at the top and in contact with all the structures placed above: this is another approximation because there is no information available on how the inner structure was constructed.

At the end, particles can exit the box by passing another window (dimensions:  $14.3 \times 12 \times 0.3\text{ cm}$ ) placed at the bottom of the box, and simulated in the code as

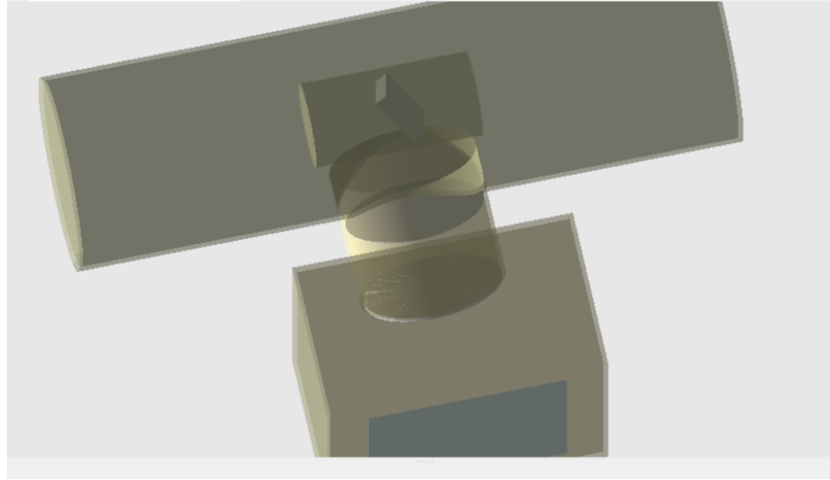


Figure 3.2: View of the interior of X-ray Tube, visualized thanks the GEANT4 OpenGL library.

made of  $C_8H_8$  plastic. These parts of the geometry were implemented in the same way for the first and second simulations, the parts that changed are: the RADCAL chamber, the height of the plexiglass table, and the cset-up for the cell cultures described below.

### Simulation of Dose measurement with the RADCAL Camera

The structure of the RADCAL chamber was implemented by combining several cylinders 3.3, following the structure already presented in the Fig. 2.3, and a polycarbonate sphere was set as the sensitive volume of the simulation, as stated in the documents. According to the construction manual, the walls of the RADCAL chamber were made of graphite. However, in the simulation they were made up of air: this choice can be justified by the fact that the RADCAL chamber provides a dose value that depends only on the energy deposition in its sensitive volume, so the external material does not provide a specific contribution to the final dose score. The ionisation chamber was then placed on a plexiglass table top, as in the measurement set-up.

### Simulation of the cell irradiation

The second geometry which has been simulated concerns the irradiation of cells 3.4: the Petri dish and its cap were modelled as two different cylinders with the same dimensions.

The Petri dish has a volume of  $5 \text{ mm cm}^3$ , the upper part was filled with air and the bottom one with the DMEM culture medium, for which a specific material was defined in the code, using the weight percentage of each DMEM components in formula.

In addition, as in the experimental configuration, inside the Petri dish and immersed in the culture medium a monolayer of cells,  $10 \mu\text{m}$  thick, was placed on the top of  $24 \times 24 \text{ mm}^2$  polycarbonate slide area. The material representing the

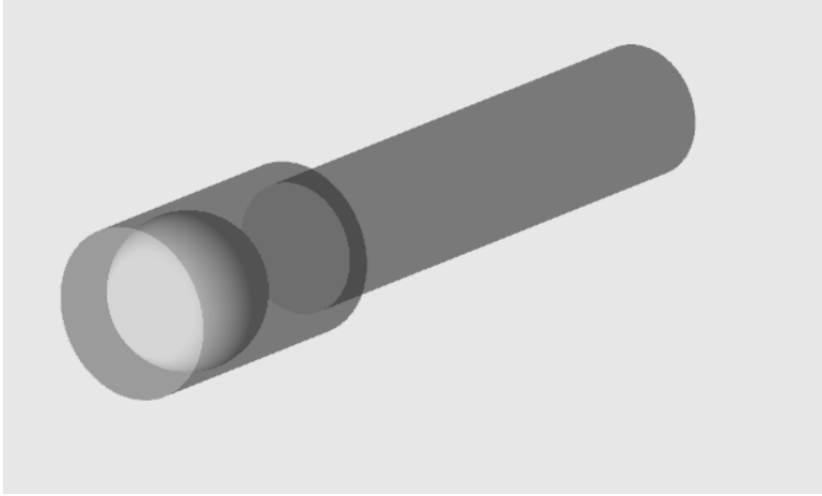


Figure 3.3: View of the RADCAL Chamber structure, visualized thanks the GEANT4 OpenGL library.

UMR106 was *soft tissue*, a specific biological material implemented in the NIST library, available in GEANT4.

### 3.1.1 Source construction and approximation

For the description of the source, located inside the machine, the available documents do not provide the exact position of the cathode and anode in the tube. The strategy adopted was to vary the position of the anode and cathode inside the glass cylinder of the X-ray tube, carrying out several tests until the results matched our expectations.

The best configuration was obtained by locating the anode in the center of the X-ray Tube and the source was set at a distance of 4 cm distance from it, along the x-axis: electrons were generated randomly over an area of 1 cm<sup>2</sup>.

The electron source energy was set at 250 keV as the tube has 250 kVp as application voltage: the Kinetic energy  $E$  of an electron of charge  $e$  is related to the voltage ( $V$ ) following the equation

$$3.1. \quad E = eV. \quad (3.1)$$

### 3.1.2 The physics list

When choosing the physics to simulate the interactions, the choice was to use a constructor already implemented in GEANT4 called G4EmStandardPhysics-option4 [49]. This constructor represents an evolution of G4EmStandardPhysics-option3 and includes some important modifications in models choice for describing electrons physics. G4EmStandardPhysics-option4 constructor was been implemented with the most accurate standard and low-energy models, to meet the demand for increasingly accurate descriptions of electron, hadron and ion tracks.

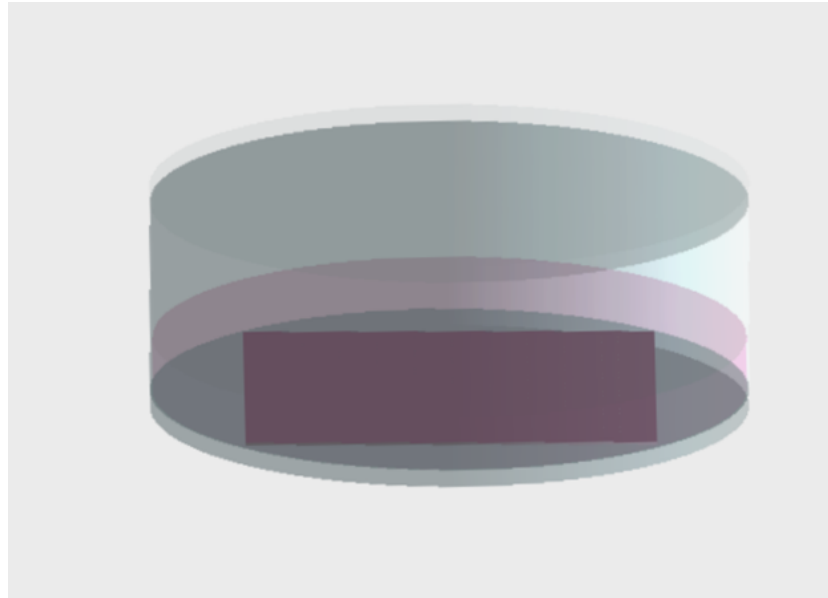


Figure 3.4: View of the Petri dish, air and DMEM medium culture, coverslip and cells seeded, visualized thanks the GEANT4 OpenGL library.

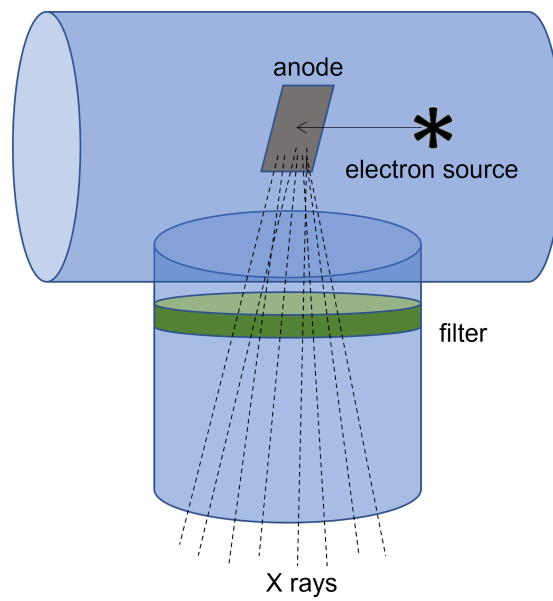


Figure 3.5: Scheme of the internal structure of the X-ray tube simulated.

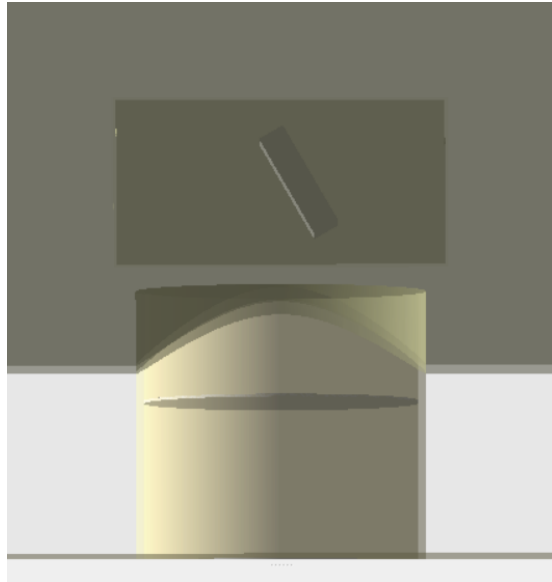


Figure 3.6: View of the internal structure of the X-ray tube, visualized thanks the GEANT4 OpenGL library.

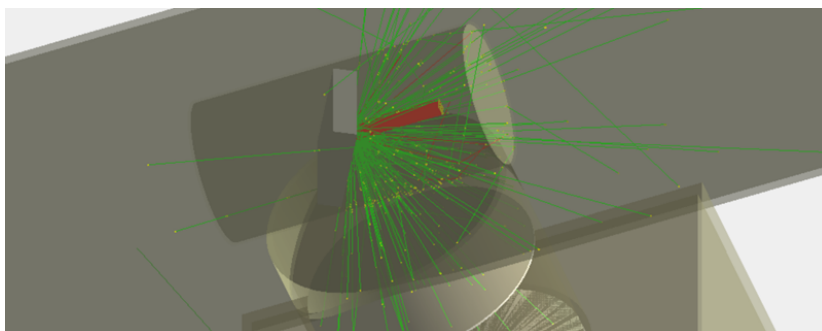


Figure 3.7: View of 100 electrons from source in red, photons produced after interactions in green and point of interactions in yellow.

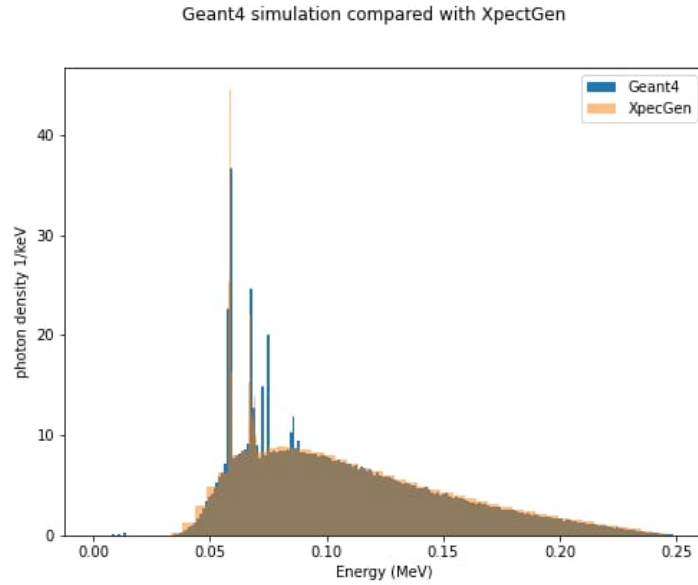


Figure 3.8: Comparison of the two different photon spectra from the GEANT4 simulation and the Xpecgen library

## 3.2 Analysis

### 3.2.1 The photon spectrum

The goal to achieve was to reproduce the photon spectrum emitted from the X-ray Tube simulated and compare it to the one generated by the Xpecgen library to validate the simulation result. In order to reproduce the spectrum, two different scoring volumes were defined: the lower plastic window of the air box, plus the RADCAL chamber sensitive volume or the cells monolayer respectively for the two situations simulated.

The operative quantities collected were the kinetic energy on these three sensitive volumes for 40 billions particle source. The representation of the irradiation simulation in both configuration set up is reported in figures 3.10 and 3.9.

In the GEANT4 simulation, the photon energy spectrum was scored in the plastic window of the air box, the most adequate condition for comparing this with the one the xpecgen library. In fact, photons which come out from the filter, pass through only a layer of air and exit from the tube interacting only with the window air box.

A chart which shows the comparison between the two energy spectrum is shown in Fig. 3.8.

The analysis for the spectra has been made using Jupyter Notebook to which the results of simulations are readable thanks the format *.csv* chosen as the output. The overlapping of the two photon spectra shows an high level of agreement and validate the GEANT4 simulation totally. This allow us to consider this results as a starting point to determine a estimate of the goodness measure that the radcal give us as a calibration of the dose received. Moreover, this agree-

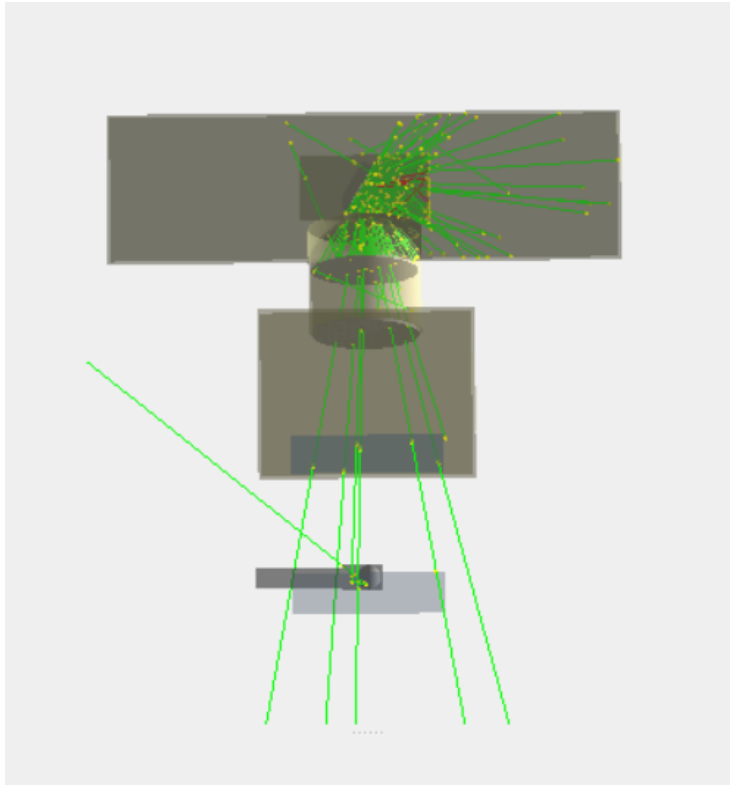


Figure 3.9: Irradiation simulation of the RADCAL geometry structure with 100 electrons from the source.

ment allows us to use this spectrum to validate the actual dose received by the cells during irradiation. In fact, the dose is prescribed to the cells according to the dose value measured by the ionization chamber, however, the cell layer may not be in charged particles equilibrium conditions, thus the calibration is not precise. The availability of a validated simulation of the entire set-up allows the verification of dose prescription and a possible introduction of correction factors. This simulation has been prepared and it is currently running: it will not be reported in this thesis.

### 3.2.2 Consideration on the calibration

Once validated the spectrum, it is possible to estimate the dose absorbed in the RADCAL sensitive volume and then compare it with the dose absorbed in the cellular layer. The parameters calculated to this end were the energy deposit for each particle step within the RADCAL sensitive volume which sum up to make the total dose. The same is performed for the evaluation in the cellular layer. The doses per source electron released in those two volumes is shown in Table 3.2.2. The dose for the cells monolayer still has a high error, which can be reduced in future simulations. Anyhow, from these simulations we can see that by considering the dose absorbed in the RADCAL as the nominal one, we are overestimating the dose to the cells by approximately 23%. This results

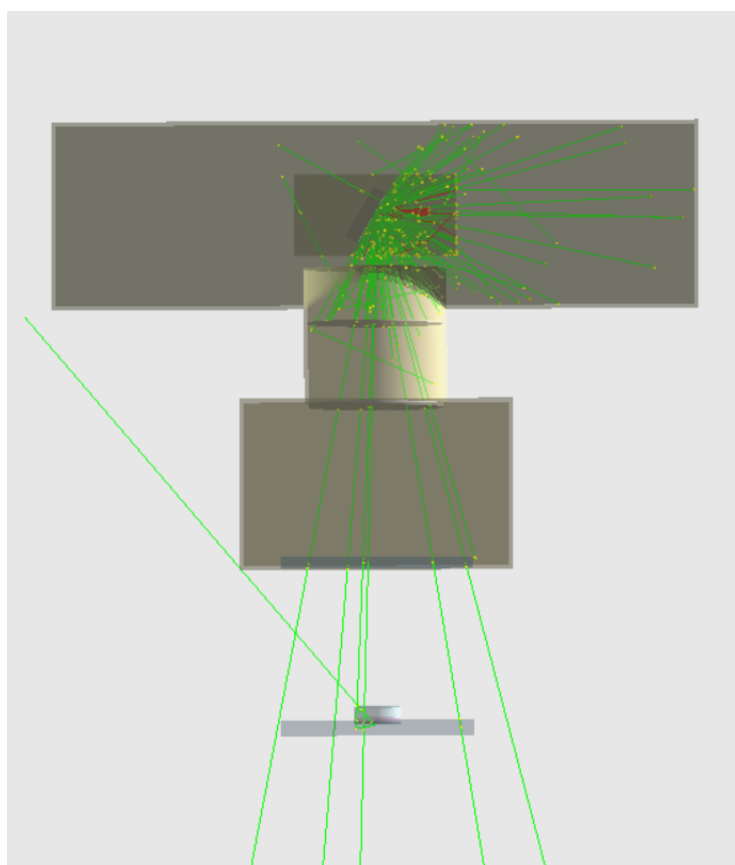


Figure 3.10: Simulation of the irradiation of the Petri dish with a cell monolayer  $10\mu\text{m}$  thick, with 100 electrons from the source.

supports the idea that further investigations have to be performed to better evaluate the absorbed dose.

Dose collected in RADCAL Sensitive volume in GEANT4 simulation
$2.75\text{e-}19 \pm 0.05\text{e-}19$ Gy/source electron
Dose collected in Cells monolayer in GEANT4 simulation
$2.1 \text{ e-}19 \pm 0.3 \text{ e-}19$ Gy/source electron

# Chapter 4

## Experimental irradiation for DNA damages studies with the foci technique

### 4.1 The foci technique

The Double Strand Breaks (DSBs) represents a modification of the DNA structure in cell which cannot always be repaired. For this reason, the DSBs play an important role in cells life because they determine the possibility of apoptosis, necrosis process or duplication with mutations which can eventually induce cancer.

Double Strand Breaks [50] are called endogenous when they are caused by the proximity of many Single Strand Breaks that may statistically occur in healthy cells, or exogenous, i.e. when caused by external agents, such as the ionizing radiation.

In eukariotic cells, two repair mechanisms were naturally developed and act depending on the type of induced DSBs and on the cell cycle stage. The *homologous recombination* that uses an intact DNA region as a copy to reconstruct the damaged part of the elic and acts in S or G2 stages, and the *non homologous end-joining*, in phase G1, which attaches the two different damaged DNA extremities, sometimes leading to chromosomic aberrations.

It was noted that after a DSB, the phosphorylation of the histone *H2AX* takes place and it assumes the form of  $\gamma - H2AX$ . The *H2AX* is made of kinases proteins as the ATM: when a damage occurs, the ATM is recalled in the damage site and this starts the phosphorylation of the *H2AX*. This stops the cell cycle, to allow some enzymes to repair the damage, suggesting that the *H2AX* plays the important role of promotion of repair and genomics stability.

We are interested in first identifying *H2AX* and then quantifying the respective shape of phosphorylation because it is closely related to the total amount of DNA damage and can give us information about the total radiation dose absorbed.

This allows to study also the damage typology and frequency at the same ab-

sorbed dose but caused by different radiations and then, ultimately it returns a biological effectiveness measure once fixed a specific DNA damage endpoint. This goal is pursued by the employ of a specific antibody who recognizes the phosphorylation, hence the damages, and the consequent repair in situ. The DNA damage site where the protein ATM acts is called focus and today the foci are studied thanks technique as cytometry [51] and Western-Blotting [52]. In these years, this research has had a huge impact in medicine [50] because the measurement of *H2AX* presence has become a reliable index to evaluate the effectiveness of radiotherapy or chemotherapy allowing the quantification of the induced DSBs. In addition, the presence of the *H2AX* in the telomeres extremity could offer a way to study the replicative senescence and determine the possibility to recognize a cancerous cell.

## 4.2 The experimental set-up

For this project, I participated in the irradiation with X-rays carried out at the biophysics laboratory in Naples in November 2022. The experiment concerned the irradiation of a rat osteosarcoma cell line (UMR106): cells were seeded and treated following a specific protocol designed for the purpose of obtaining data to be compared with future simulations. The irradiation of this culture was aimed at detecting and studying the phosphorylation of the *H2AX* gene, which takes on the configuration of  $\gamma$ -*H2AX* determining the formation of a focus, and at correlating the number of foci with the quantity of DSBs in the cells. In order to study these effects, two time endpoints were set at 30 minutes and 24 hours after the irradiation.

### 4.2.1 Preliminary phase

The cells were prepared the day before irradiation and seeded in an amount of 10,000 for the cultures that would be studied at 24 h and 15,000 for the cultures at 30 min. This difference is necessary to take into account the biological response to the irradiation. Generally, cells that are damaged, activate repair mechanisms that significantly affect their survival: longer times give the cells more time to repair and a greater chance of survival (considering just this one as the parameter to control), whereas shorter times give a different picture in which the damage significantly affects the cell population because they do not have the time to activate all the mechanisms. This is why a higher number of cells are seeded for the first endpoint, making it possible to obtain good statistics for the results while allowing a comparison with other samples.

Prior to irradiation, the cells are seeded on a glass cover slip, which is placed inside a 35 mm Petri dish. The cells remain submerged within the culture medium by a volume of 3 ml total (medium+cells), and this is the condition of the irradiation.

### 4.2.2 The irradiation

The irradiation has been performed with the X-Ray Tube STABILIPAN, TR300F, described in Chapter 2 and it was organized in two runs: the total dose delivered for every irradiation was set taking into account the calibration, obtained

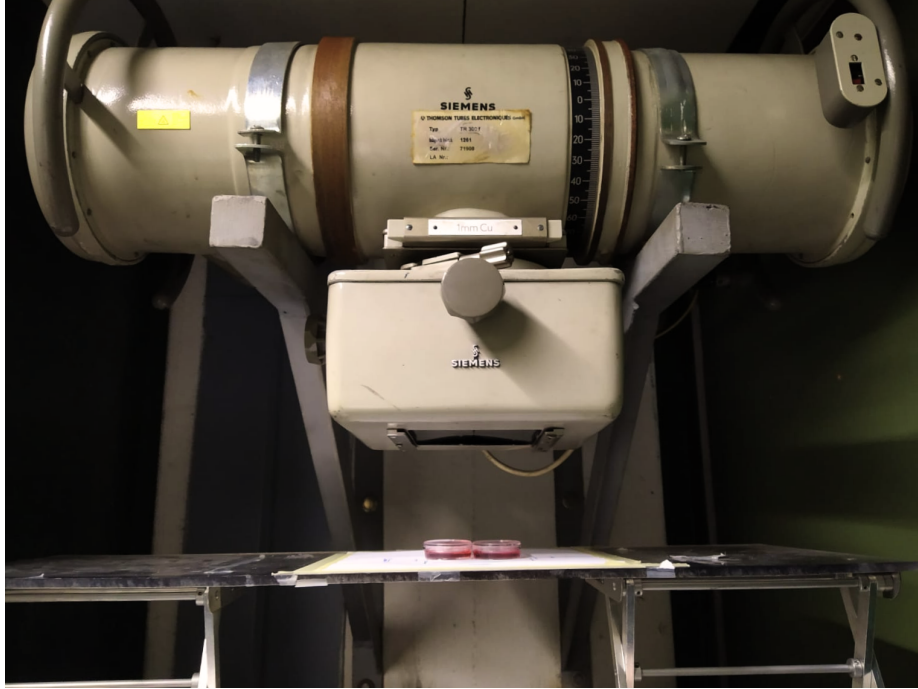


Figure 4.1: The STAPILIPAN X-rays tube and the experimental configuration adopted in November 2022, Naples.

with the RADCAL ionization chamber. In particular, the calibration delivered a dose rate of  $1.37 \text{ Gy}/\text{min}$  and thus the irradiation time was 21.90 sec for the nominal dose 0.5 Gy and 88 sec for 2 Gy. Sample preparation and dose delivered values are summarized in Table 4.2.2.

Number of Cells	Time End-points	Dose (Gy)
15000	30min	0.5 and 2
10000	24h	0.5 and 2

The experimental configuration adopted for each run is reported in Fig. 4.1 and 4.2: the Petri dishes were placed on the plexiglass plate to make sure that the total dose delivered to cultures was the same.

After the irradiation, the cultures were stored inside an incubator: then the first three dishes were selected for the 30 minute endpoint.

The three dishes Fig. 4.3 were the two irradiated with the 0.5 and 2 Gy and one more which was the sham-irradiated control: it offered a comparison and gave information about the cells health and possible contamination. In addition, it allowed monitoring the culture behavior during all the protocol.

### 4.2.3 Protocol application

The stages of the protocol are organized in five phases:



Figure 4.2: The Petri dishes with the UMR106 cells before the irradiation, placed below the X-ray Tube, November 2022, Naples.

### Fixation

The culture medium is removed from the Petri and the cells are first washed and then added with paraformaldehyde. This works as a biological fixative so it is able to inhibit cell degradation due to the possible breakdown of enzymes or bacterial replications, it serves to preserve the sample which is then placed at 4 degrees before proceeding with the second phase.

### Permeabilization

After further washing, a permeabilization buffer is added to the cells to fix and permeabilize the cells before intracellular staining of cytokines and other cytoplasmic and/or nuclear antigens. This solution [53] allows reducing the non-specific staining of fluorochrome-labelled antibodies and increase the signal-to-noise ratio of fluorescence.

### Blocking

In this phase, the most important role is played by the administration of the blocking buffer [54]: in fact, before moving on to the fourth phase that involves the use of antibodies that detect the membrane proteins, it is important that the surface with the binding site of the cell is blocked, i.e. that a possible linking of antibodies to the sites which initially served to immobilize the proteins of interest is avoided. If this happens, it is called *non-specific antibody binding*.

### Antibody phase

The antibody stage, is further subdivided in two sub-stages, according to the antibody used.

The role of an antibody is to link to a specific membrane protein and, for this



Figure 4.3: The three Petri dishes for the 30 minutes endpoint, November 2022, Naples.



Figure 4.4: Pictures taken during the fixation phase, November 2022, Naples.

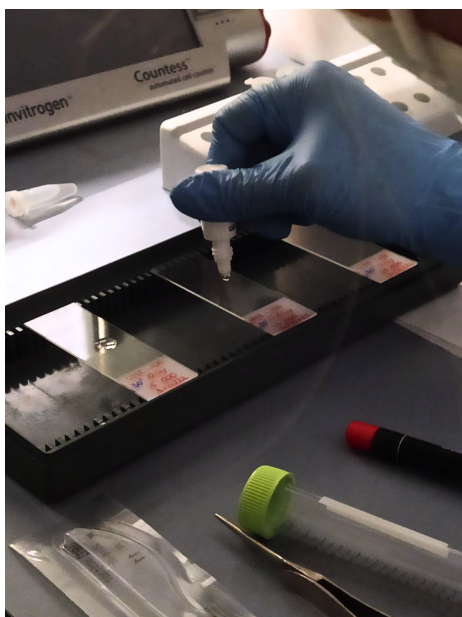


Figure 4.5: Posthybridization phase, adding of Prolong Gold antifade with DAPI. November 2022, Naples.

experiment, an antibody able to recognize  $\gamma - H2AX$  and to make it visible was needed. At least two different antibody types must be used: the first for identifying the protein and reach it, the second for recognizing the sites where the first antibody and the protein were located. Therefore, if the first is crucial for individualize the damages, the latter is determinant for increasing the detection technique sensitivity.

For this specific protocol two primary antibodies **Anti  $\gamma H2AX$  + Anti 53BP1** able to highlight the protein presence were chosen, while the secondaries were the **Anti-mouse+Anti-rabbit**. To use the secondaries it was important to not work under light in order not to deteriorate the molecular complexes, so all of the work was done in a dark room.

#### Posthybridization

This is the last stage and it requires the removal of cells from each coverslip and their accommodation on other sterile cover glasses where a drop of **Prolong Gold antifade with DAPI** was added "to preserve the signals of the target molecules for long-term storage and analysis [55]".

After one night, or about 12 hours stored in the dark and at room temperature, the preservation of cells takes place in a freezer, at  $-20^{\circ}C$ : in this way, once damages have been fixed, they can be studied at any time.

### 4.3 Experimental Results

One of the possible analysis techniques was fluorescence microscopy, which exploits the ability of molecular compounds to re-emit light when properly excited.

The molecules which are chemically linked to secondary antibodies and that reached the site of damage with them are fluorophores, compounds that can re-emit light following excitation by light sources.

Since the fluorophore is located at the damage site, once the light sites present in the target have been quantified, it will be possible to determine an estimate of the total damage present in the samples using a fluorescence microscope.

For the analysis of these first data, a technique called *colocalization* [56] was chosen: it allowed us to study a possible spatial correlation of several fluorescent spots in the same target that are located very close together but which emit at different wavelengths and are, therefore, easily distinguishable. In this specific case, colocalization has represented the best choice as it was not possible to rely on signals from localization of *H2AX* phosphorylation sites since these could have provided an overestimation of the DNA damage present. The antibody used for  $\gamma$  - *H2AX* detection could be responsible for possible non-specific binding that produces light spots even when no double strand breaks have occurred.

For this reason, the most suitable choice was to associate the  $\gamma$  - *H2AX* signals with those emitted by the presence of the *53bp1* protein [57]. This particular molecular complex is invoked at the site of damage in case of double strand breaks and collaborates with other enzymes in choosing the best repair pathway for the cell, depending on the stage of the cell life cycle and on the extent of the damage. The *53bp1*, in particular, reaches higher concentrations when damage occurs in the G1 phase<sup>1</sup> and promotes the choice of the non-end joining recombination pathway.

According to that, a fluorescence microscope was used to determine the sites of damage from which a light signal originated, for the two samples at 30 minutes post-irradiation, at the absorbed dose of 0.5 and 2 Gy and the control sample. The analysis was performed on 50 cells using the software coupled to the microscope; an average of the two different numbers of light spots was determined. The chart in Fig. 4.6 shows the average number of colocalizations as a function of the dose.

Results show that, as the dose administered increases, the number of damages also increases, as expected.

The choice of 30 minutes, as the first endpoint of analysis, is not coincidental: studies [50] propose that it is only after this time interval that the most amount of foci is present. It is important to note that several factors influence the kinetics foci formation and their loss, which is why further studies at different time endpoints are needed. More data regarding other measurements campaigns and different endpoints, deep biological interpretation and analysis as a function of absorbed dose and elapsed time are beyond the scope of this work and will be extensively described in the MSc thesis by Alessia Fornaro, biologist at the University of Naples.

---

<sup>1</sup>G1 phase is a living cell cycle in which cells synthesize a protein required for the DNA synthesis and mRNA

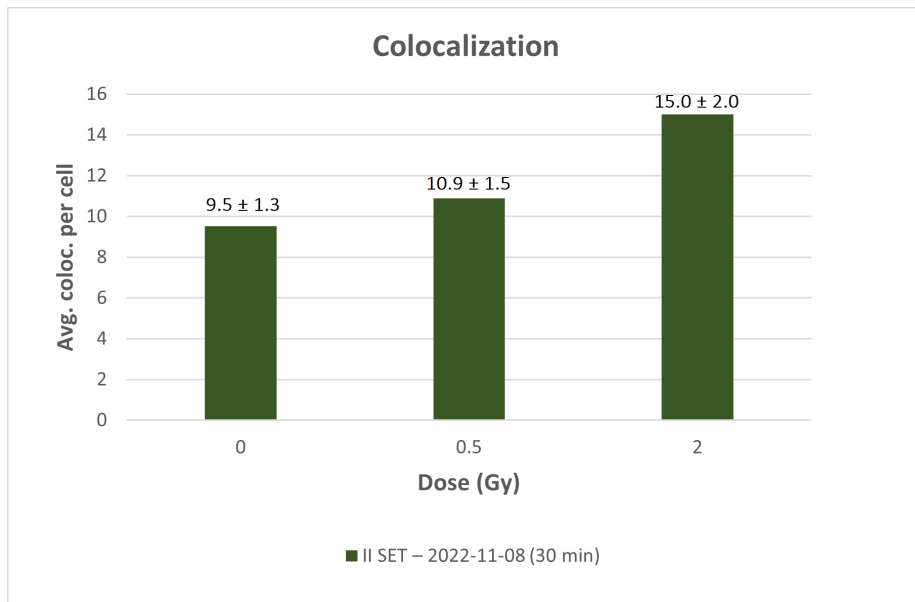


Figure 4.6: Chart of average colocalization in function of dose, light spots of  $\gamma - H2AX$  phosphorylation counted in 50 cells (Courtesy of Alessia Fornaro, University of Naples).

# Chapter 5

## Conclusions and future perspectives

This thesis represents the preliminary stage necessary to achieve the goals of a broader project which is framed in the BNCT research line. The context is the possibility to combine Monte Carlo detailed dosimetry and radiobiologica measurement to deepen the knowledge of the dose-effect relation in BNCT. In particular, an activity has been recently started in Pavia, aimed at using GEANT4 to simulate the dosimetry in cells due to BNCT, neutron and photon irradiation, and to reproduce the subcellular damage via Monte Carlo simulation. This will produce new knowledge on the effects of a mixed-field radiation (typical in BNCT) at the level of cell DNA. The Pavia research group has thus started to use the Monte Carlo software GEANT4. Before reaching the stage of sub-cellular radiobiology simulation, preliminary studies are necessary to know advantages and limitations, strengths and weaknesses of this new approach. This thesis has dealt with an extensive learning and research work, leading to the capacity of reproducing one of the irradiation sources used for radiobiological studies: the X-Ray tube. The possibility of working with an open-source toolkit ensured the instruments for the construction of our application and offered the possibility of a continuous comparison to continuously improve the simulations.

One decisive instrument was the *baltig* platform: we have exploited its environment to initiate online content sharing within the research group, in which changes could be shared in real-time, making it possible to continue the work faster and easier. This implementation is particularly meaningful considering that this was the starting point of a study that will likely be followed by other researchers, who will be able to access the results and the codes smoothly. In fact, it was possible to store in the platform the different files, making changes and uploading the content with comments. This made it possible to keep track of the path taken, which was not always linear.

The work presented in this thesis consists of extensive testing work on the code to improve its performance. The results respond to the goal of producing a reliable simulation tool for the spectrum of the radiogenic machine. Inside the open-source perspective of GEANT4, the XrayTube code also provides the tools

for any GEANT4 user application developers to build their photon irradiation machine, offering as a ready-made software or a starting point for further customization.

The fourth Chapter of this work, has been devoted to an experimental measurement. The possibility to attend the measurement campaign at the University of Naples offered the opportunity to examine the operating manuals of that Stabilipan tube, understand its structure, and implement the details in the simulation.

Moreover, this experience represented the other side of the dose-effect studies: the radiobiological measurements *in-vitro*. The cell irradiation performed in November 2022 was one of the multiple campaigns that must be carried out to produce a reliable series of biological data regarding the effects in cells as a function of the type of radiation and of the absorbed dose. It is in fact the starting point for testing the simulation toolkit developed in this thesis. The results obtained and presented here show that XrayTube returns a reliable output to simulate the spectrum of the machine. Furthermore, it offers a tool for the verification of the nominal dose prescribed to the cell cultures. In fact, the dose absorbed in a small volume such as the cell layer, is influenced by the lack of equilibrium of charged particles. The irradiation of a volume which is sensibly different than the detector used to calibrate the system may introduce a systematic error in the evaluation of dose delivered to cells. The Monte Carlo model, once validated, is a powerful tool to apply correction to the nominal dose values. Finally, the obtained spectra will become the input for subsequent simulations, to model the cell damage. Within the GEANT4 toolkit, the GEANT4-DNA extension offers a way to study the interactions of radiation with the matter on the micrometer and nanometric scale: having an input that communicates directly with GEANT4-DNA will be crucial for reproducing the cell damages. In the future it will be possible to further improve this instrument, thanks to the flexibility of object-oriented programming, with the aim of reproducing new experimental conditions and predicting cell-damage.

The XrayTube tools can be found within this repository github link:

**<https://github.com/ipostuma/XrayTube>**

# Ringraziamenti

Vorrei dedicare questo spazio per ringraziare tutti coloro dei quali aiuto e supporto sono stati determinanti per la realizzazione di questo lavoro. Le prime parole che desidero spendere sono per il mio relatore, il Dott. Ian Postuma e per la Professoressa Silva Bortolussi, correlatrice dell'elaborato ma senza la quale non sarebbe stato possibile iniziare questo percorso.

Ringrazio Ian consapevole che non sarà possibile racchiudere in poche righe l'enorme senso di gratitudine che provo nei tuoi confronti: grazie per avermi mostrato e insegnato come lavorare, per avermi permesso di restare al tuo fianco per imparare qualcosa di totalmente nuovo e affascinante e per aver portato pazienza riguardo le mie innumerevoli domande, trovando sempre il modo migliore per farmi imparare qualcosa. Grazie per aver scommesso su di me e scelto di supportarmi anche quando la fortuna e le tempistiche non sono state proprio dalla nostra parte e grazie, inatteso ma dovuto, anche per avermi nuovamente fatto apprezzare la programmazione, strada che avevo scelto di non voler più percorrere qualche anno fa ma che mi ha regalato delle soddisfazioni incredibili durante tutto il percorso di tesi e con la quale ho avuto modo, un po' di più, di conoscere me stessa.

Ringrazio Silva per avermi dato la possibilità di lavorare all'interno di questo gruppo incredibile, facendomi sentire parte attiva di questo progetto, eliminando le distanze tra studente e insegnante e offrendomi l'opportunità di continui confronti. Grazie per avermi regalato delle vere e proprie esperienze di vita come quella presso l'Università di Napoli, con la quale ho avuto modo di inserire un'esperienza sperimentale come tassello della mia formazione, e la possibilità di contattare il professor Mairani per il mio prossimo soggiorno ad Heidelberg. Grazie per tutto il tempo che hai dedicato all'ascolto dei miei dubbi, ai consigli importanti che mi hai donato, di cui ho fatto e farò ancora tesoro, e per avermi offerto l'occasione di mettere in gioco me stessa per riuscire a capire cosa tanto desidero.

Vi ringrazio per aver fatto il possibile e compiuto anche l'impossibile per la realizzazione di questa tesi, è stata un'esperienza indimenticabile che porterò per sempre con me come una delle più arricchenti che abbia mai fatto.

Ci tengo a ringraziare i miei genitori che hanno sempre mostrato estrema fiducia nelle mie scelte, permettendomi così di vivere a mille chilometri da casa e lavorare su ciò che realmente ho amato. Grazie, Mamma e Papà, per avermi ascoltata ed essere stati un punto di riferimento, un porto sicuro e una spinta anche quando la mancanza era tanta e la voglia di tornare interagiva con i miei obiettivi.

Ringrazio mia sorella, un altro perno della mia vita, la mia esatta metà e parte complementare. Il mio orgoglio più grande e per la quale nessuna parola sarà sufficiente per esprimere quanto per me tu sia stata fondamentale nella realizzazione di tutto questo, e non solo.

Grazie ai miei Amici, Sara che instancabilmente mi è rimasta a fianco offrendomi ogni volta la prospettiva giusta con cui poter guardare le cose, Leo che da 15 anni sopporta il mio caratteraccio e Daniele che trova sempre un momento per me. Grazie per la vostra leggerezza e buon umore, per esservi fidati di me e avermi appoggiata. Siete le persone migliori che potessi sperare di avere al mio fianco.

Grazie anche a Erica, Francesco e Matilde il quale supporto reciproco ha reso la nostra esperienza divertente e unica. Grazie per la vostra presenza anche adesso che vi trovate così tanto fisicamente distanti, grazie Francesco per le chiamate notturne, Erica per l'ordine che sai mettere ai miei pensieri e Matilde per la sincerità delle tue opinioni. Spero di poter lavorare ancora insieme in un futuro prossimo e condividere momenti tanto belli come quelli trascorsi in questi mesi.

Grazie ad Aurora, mia coinquilina e amica, per avermi fatto vivere Pavia in modo totalmente inaspettato, avermi offerto conforto, amicizia, esperienze ed essermi stata vicino in ogni momento. Grazie per avermi letteralmente offerto rifugio, sia fisico che morale quando più ero debole.

E sicuramente non posso non ringraziare Giulia, Valentina e Lucia che mi hanno accolta in casa loro in questi ultimi mesi, hanno rispettato i miei spazi e dato la possibilità di essere ascoltata. Siete tre ragazze incredibili e mi sento davvero fortunata per aver avuto modo di conoscervi.

E grazie anche a Rossella, Roberta, Marco, Giuseppe, Bruno, Irene ed Enrica, da anni al mio fianco e chissà per quanti altri ancora.

Ancora una volta, perché credo di averlo detto un milione di volte ma scritto solo 19, **grazie, di cuore.**

# Bibliography

- [1] A. M. D. Viegas, I. Postuma, S. Bortolussi, C. Guidi, J. S. Riback, L. Provenzano, B. Marcaccio, A. E. Rossini, C. Ferrari, L. Cansolino, *et al.*, “Detailed dosimetry calculation for in-vitro experiments and its impact on clinical bnct,” *Physica Medica*, vol. 89, pp. 282–292, 2021.
- [2] “Umr-106 cell line.” <https://www.atcc.org/products/crl-1661>, consulted the 26-01-2023.
- [3] S. Bortolussi, I. Postuma, N. Protti, L. Provenzano, C. Ferrari, L. Cansolino, P. Dionigi, O. Galasso, G. Gasparini, S. Altieri, *et al.*, “Understanding the potentiality of accelerator based-boron neutron capture therapy for osteosarcoma: dosimetry assessment based on the reported clinical experience,” *Radiation Oncology*, vol. 12, no. 1, p. 130, 2017.
- [4] F. H. Attix, *Introduction to radiological physics and radiation dosimetry*. John Wiley & Sons, 2008.
- [5] R. J. da Cruz Roque, *X-ray imaging using 100  $\mu\text{m}$  thick Gas Electron Multipliers operating in Kr-CO<sub>2</sub> mixtures*. PhD thesis, MA thesis. Universidade de Coimbra, 2018.
- [6] F. Delvillani, “What does dna look like?.” <https://www.biopills.net/dna/>, consulted the 12-02-2023.
- [7] A. L. Hub, “Where is dna found in a cell?.” <https://www.ancestry.com/c/dna-learning-hub/cells>, consulted the 12-02-2023.
- [8] J. S. de Souza, “The chromatina.” <https://www.infoescola.com/genetica/cromatina/>, consulted the 12-02-2023.
- [9] I. Foffa, M. Cresci, and M. G. Andreassi, “Health risk and biological effects of cardiac ionising imaging: From epidemiology to genes,” *International journal of environmental research and public health*, vol. 6, pp. 1882–93, 07 2009.
- [10] G. B. Avery, “The biological effects of ionizing radiation.” *Clinical proceedings - Children’s Hospital of the District of Columbia*, vol. 17, pp. 146–50, 1961.

- [11] H. Song, S. Senthamizhchelvan, R. F. Hobbs, and G. Sgouros, “Alpha particle emitter radiolabeled antibody for metastatic cancer: what can we learn from heavy ion beam radiobiology?,” *Antibodies*, vol. 1, no. 2, pp. 124–148, 2012.
- [12] C. J. W. (editor), “Mcnp users manual - code version 6.2,” *Los Alamos National Laboratory, Los Alamos, NM, report LA-UR-17-29981*, 2017.
- [13] K. P. Chatzipapas, P. Papadimitroulas, D. Emfietzoglou, S. A. Kalospyros, M. Hada, A. G. Georgakilas, and G. C. Kagadis, “Ionizing radiation and complex dna damage: Quantifying the radiobiological damage using monte carlo simulations,” *Cancers*, vol. 12, no. 4, p. 799, 2020.
- [14] P. Phruksarojanakun and P. P. Wilson, “Biased reaction branching variance reduction for monte carlo isotopic inventory methods,” *Transactions of the American Nuclear Society*, vol. 93, pp. 566–567, 2005.
- [15] S. Incerti, I. Kyriakou, M. Bernal, M. Bordage, Z. Francis, S. Guatelli, V. Ivanchenko, M. Karamitros, N. Lampe, S. B. Lee, *et al.*, “Geant4-dna example applications for track structure simulations in liquid water: A report from the geant4-dna project,” *Medical physics*, vol. 45, no. 8, pp. e722–e739, 2018.
- [16] I. Kyriakou, D. Sakata, H. N. Tran, Y. Perrot, W.-G. Shin, N. Lampe, S. Zein, M. C. Bordage, S. Guatelli, C. Villagrasa, *et al.*, “Review of the geant4-dna simulation toolkit for radiobiological applications at the cellular and dna level,” *Cancers*, vol. 14, no. 1, p. 35, 2021.
- [17] G. Collaboration, S. Agostinelli, *et al.*, “Geant4—a simulation toolkit,” *Nucl. Instrum. Meth. A*, vol. 506, no. 25, p. 0, 2003.
- [18] G. Collaboration, “Introduction to geant4,” 2021.
- [19] K. Amako, for the Geant4 Collaboration, *et al.*, “Present status of geant4,” *Nuclear Instruments and Methods in Physics Research Section A: Accelerators, Spectrometers, Detectors and Associated Equipment*, vol. 453, no. 1-2, pp. 455–460, 2000.
- [20] J. M. Ortega, *Introduction to FORTRAN 90 for Scientific Computing*. Oxford University Press, Inc., 1994.
- [21] J. Allison, K. Amako, J. Apostolakis, P. Arce, M. Asai, T. Aso, E. Bagli, A. Bagulya, S. Banerjee, G. Barrand, *et al.*, “Recent developments in geant4,” *Nuclear instruments and methods in physics research section A: Accelerators, Spectrometers, Detectors and Associated Equipment*, vol. 835, pp. 186–225, 2016.
- [22] B. Stroustrup, *The C++ programming language*. Pearson Education, 2013.
- [23] G. Cosmo, “The b1 example.” <https://gitlab.cern.ch/geant4/geant4/-/blob/master/examples/basic/B1>, consulted the 07-02-2023.
- [24] V. Ivanchenko, *Experimental Physics List Experimental Physics List QBBC*. Slide, 10th Geant4 Workshop, 9 Geant4 Workshop, 9-14 October, Lisbon, Portugal, 2006.

- [25] “Geant4 hadronic models.” [https://11r.in2p3.fr/activites/physique/atf2/Geant4\\_hadronic\\_models.html](https://11r.in2p3.fr/activites/physique/atf2/Geant4_hadronic_models.html).
- [26] T. Kluyver, B. Ragan-Kelley, F. Pérez, B. Granger, M. Bussonnier, J. Frederic, K. Kelley, J. Hamrick, J. Grout, S. Corlay, P. Ivanov, D. Avila, S. Abdalla, and C. Willing, “Jupyter notebooks – a publishing format for reproducible computational workflows,” in *Positioning and Power in Academic Publishing: Players, Agents and Agendas* (F. Loizides and B. Schmidt, eds.), pp. 87 – 90, IOS Press, 2016.
- [27] C. R. Harris, K. J. Millman, S. J. van der Walt, R. Gommers, P. Virtanen, D. Cournapeau, E. Wieser, J. Taylor, S. Berg, N. J. Smith, R. Kern, M. Picus, S. Hoyer, M. H. van Kerkwijk, M. Brett, A. Haldane, J. Fernández del Río, M. Wiebe, P. Peterson, P. Gérard-Marchant, K. Sheppard, T. Reddy, W. Weckesser, H. Abbasi, C. Gohlke, and T. E. Oliphant, “Array programming with NumPy,” *Nature*, vol. 585, p. 357–362, 2020.
- [28] T. A. Caswell, A. Lee, E. S. de Andrade, M. Droettboom, T. Hoffmann, J. Klymak, J. Hunter, E. Firing, D. Stansby, N. Varoquaux, J. H. Nielsen, B. Root, R. May, P. Elson, J. K. Seppänen, J.-J. Lee, D. Dale, O. Gustafsson, hannah, D. McDougall, A. Straw, P. Hobson, G. Lucas, C. Gohlke, A. F. Vincent, T. S. Yu, E. Ma, S. Silvester, C. Moad, and K. Sunden, “matplotlib/matplotlib: Rel: v3.7.0,” Feb. 2023.
- [29] S. Incerti, G. Baldacchino, M. Bernal, R. Capra, C. Champion, Z. Francis, P. Gueye, A. Mantero, B. Mascialino, P. Moretto, *et al.*, “The geant4-dna project,” *International Journal of Modeling, Simulation, and Scientific Computing*, vol. 1, no. 02, pp. 157–178, 2010.
- [30] P. Arce, D. Bolst, M.-C. Bordage, J. Brown, P. Cirrone, M. A. Cortés-Giraldo, D. Cutajar, G. Cuttone, L. Desorgher, P. Dondero, *et al.*, “Report on g4-med, a geant4 benchmarking system for medical physics applications developed by the geant4 medical simulation benchmarking group,” *Medical physics*, vol. 48, no. 1, pp. 19–56, 2021.
- [31] S. Incerti, M. Douglass, S. Penfold, S. Guatelli, and E. Bezak, “Review of geant4-dna applications for micro and nanoscale simulations,” *Physica Medica*, vol. 32, no. 10, pp. 1187–1200, 2016.
- [32] T. NIST, “National institute of standard and technologies.” <https://www.nist.gov>, consulted the 12-02-2023.
- [33] ICRU, “International commission on radiation units and measurements.” <https://www.icru.org>, consulted the 12-02-2023.
- [34] Z.-H. Loh, G. Doumy, C. Arnold, L. Kjellsson, S. Southworth, A. Al Hadad, Y. Kumagai, M.-F. Tu, P. Ho, A. March, *et al.*, “Observation of the fastest chemical processes in the radiolysis of water,” *Science*, vol. 367, no. 6474, pp. 179–182, 2020.
- [35] M. A. Bernal, M. C. Bordage, J. M. C. Brown, M. Davidková, E. Delage, Z. El Bitar, S. A. Enger, Z. Francis, S. Guatelli, V. N. Ivanchenko, *et al.*, “Track structure modeling in liquid water: A review of the geant4-dna very

- low energy extension of the geant4 monte carlo simulation toolkit,” *Physica Medica*, vol. 31, no. 8, pp. 861–874, 2015.
- [36] M. Karamitros, S. Luan, M. A. Bernal, J. Allison, G. Baldacchino, M. Davidkova, Z. Francis, W. Friedland, V. Ivantchenko, A. Ivantchenko, *et al.*, “Diffusion-controlled reactions modeling in geant4-dna,” *Journal of Computational Physics*, vol. 274, pp. 841–882, 2014.
- [37] S. Uehara and H. Nikjoo, “Monte carlo simulation of water radiolysis for low-energy charged particles,” *Journal of radiation research*, vol. 47, no. 1, pp. 69–81, 2006.
- [38] Z. Francis, S. Incerti, V. Ivanchenko, C. Champion, M. Karamitros, M. Bernal, , and Z. El Bitar, “Monte carlo simulation of energy-deposit clustering for ions of the same let in liquid water,” *Physics in Medicine & Biology*, vol. 57, no. 1, p. 209, 2011.
- [39] M. Ester, H.-P. Kriegel, J. Sander, X. Xu, *et al.*, “A density-based algorithm for discovering clusters in large spatial databases with noise.,” vol. 96, no. 34, pp. 226–231, 1996.
- [40] M. A. Bernal, D. Sikansi, F. Cavalcante, S. Incerti, C. Champion, V. Ivanchenko, and Z. Francis, “An atomistic geometrical model of the b-dna configuration for dna–radiation interaction simulations,” *Computer Physics Communications*, vol. 184, no. 12, pp. 2840–2847, 2013.
- [41] S. Incerti, C. Champion, H. Tran, M. Karamitros, M. Bernal, Z. Francis, V. Ivanchenko, A. Mantero, G.-D. collaboration, *et al.*, “Energy deposition in small-scale targets of liquid water using the very low energy electromagnetic physics processes of the geant4 toolkit,” *Nuclear Instruments and Methods in Physics Research Section B: Beam Interactions with Materials and Atoms*, vol. 306, pp. 158–164, 2013.
- [42] C. Villagrasa, “The wolenucleardna example.” <http://geant4-dna.in2p3.fr/resources/TN-wholeNuclearDNA.pdf>, consulted the 12-02-2023.
- [43] E. Delage, “The pdb4dna example.” <http://pdb4dna.in2p3.fr>, consulted the 12-02-2023.
- [44] R. Corporation, “The radcla ionization chamber.” <https://radcal.com/10x6-6-general-purpose-ion-chamber>.
- [45] G. Hernández and F. Fernández, “A model of tungsten anode x-ray spectra,” *Medical physics*, vol. 43, no. 8Part1, pp. 4655–4664, 2016.
- [46] G. Hernández and F. Fernández, “xpecgen: A program to calculate x-ray spectra generated in tungsten anodes,” *J. Open Source Softw.*, vol. 1, no. 7, p. 62, 2016.
- [47] G. Collaboration, “Geant4 user’s guide for application developers,” *Accessible from the GEANT4 web page [1] Version geant4*, vol. 9, 2012.

- [48] P. M. Mondalek, T. W. Phillips, E. G. Randolph, and K. J. Tolly, "Design and beam characteristics of the siemens stabilipan orthovoltage unit for intraoperative radiation therapy," *Medical Dosimetry*, vol. 13, no. 1, pp. 1–6, 1988.
- [49] G. Collaboration, "Book for application developers." <https://geant4-userdoc.web.cern.ch/UsersGuides/ForApplicationDeveloper/html/index.html#>.
- [50] K. Rothkamm and S. Horn, "gamma-h2ax as protein biomarker for radiation exposure," *Ann Ist Super Sanita*, vol. 45, no. 3, pp. 265–71, 2009.
- [51] A. Adan, G. Alizada, Y. Kiraz, Y. Baran, and A. Nalbant, "Flow cytometry: basic principles and applications," *Critical reviews in biotechnology*, vol. 37, no. 2, pp. 163–176, 2017.
- [52] B. T. Kurien and R. H. Scofield, "Western blotting," *Methods*, vol. 38, no. 4, pp. 283–293, 2006.
- [53] T. F. Scientific, "ebioscience™ permeabilization buffer." <https://www.thermofisher.com/order/catalog/product/00-8333-56>.
- [54] T. F. Scientific, "ebioscience™ blocking buffer." <https://www.thermofisher.com/it/en/home/life-science/protein-biology/protein-biology-learning-center/protein-biology-resource-library/pierce-protein-methods/blocking-buffers-western-blot-elisa.html>.
- [55] T. F. Scientific, "ebioscience™ prolong antifade." <https://www.thermofisher.com/it/en/home/life-science/cell-analysis/cellular-imaging/fluorescence-microscopy-and-immunofluorescence-if/mounting-medium-antifades/>.
- [56] J. W. Comeau, S. Costantino, and P. W. Wiseman, "A guide to accurate fluorescence microscopy colocalization measurements," *Biophysical journal*, vol. 91, no. 12, pp. 4611–4622, 2006.
- [57] M. Mirza-Aghazadeh-Attari, A. Mohammadzadeh, B. Yousefi, A. Mihanfar, A. Karimian, and M. Majidinia, "53bp1: A key player of dna damage response with critical functions in cancer," *DNA repair*, vol. 73, pp. 110–119, 2019.